



OPEN

Advances in the greener synthesis of chromopyrimidine derivatives by a multicomponent tandem oxidation process

Pouya Ghamari Kargar[✉] & Ghodsieh Bagherzade[✉]

A hydrophilic cobalt/copper heterogeneous bimetallic catalyst named mTEG-CS-Co/Cu-Schiff-base/IL was successfully synthesized from chitosan polysaccharide. The new catalyst was investigated and confirmed using various techniques including FT-IR, FE-SEM, EDX-EDS, XRD, TEM, TGA, AFM, NMR and ICP. The catalyst exhibited powerful catalyst activity for the tandem one pot oxidative chromopyrimidine reaction from benzyl alcohols under mild conditions, utilizing air as a clean source in a green protocol. The catalyst was compatible with a wide range of benzyl alcohols, and aldehydes formed in situ, and bis-aldehydes synthesized were condensed with urea/4-hydroxycumarin to provide favorable products in good yields for all derivatives (14 new derivatives). The presence of tri-ethylene glycol and imidazolium moieties with hydrophilic properties on the mTEG-CS-Co/Cu-Schiff-base/IL nanohybrid provides dispersion of the nanohybrid particles in water, leading to higher catalytic performance. Furthermore, the reaction exhibited several other notable features, including low catalyst loading, the ability to be recycled for up to 6 stages, high atom economy, a simple work procedure, short reaction time, utilization of an environmentally friendly nanohybrid, and the replacement of volatile and organic solvents with water solvent.

Sustainable and green chemistry aims to develop environmentally friendly methods for synthesizing biologically significant compounds, such as heterocyclic compounds^{1,2}. The development of cost-effective and reliable methodologies is crucial for the sustainability of green chemistry, the use of benign solvents, and the expansion of less toxic and promising catalysts^{3,4}. Heterocyclic compounds are molecules with cyclic structures that contain at least one atom, such as S, O, or N in addition to carbon^{5,6}. These compounds have diverse pharmacological properties and are used clinically. Pharmacologically, they inhibit simple voltage-gated receptors and modulate highly complex signaling cascades in cells^{7,8}. Among the heterocycles containing nitrogen, oxygen, and sulfur, chromenes and pyrimidines are important classes of heterocyclic compounds. Many drugs and bioactive natural products contain pyrimidine and chromene as privileged moieties⁹⁻¹¹.

The pyrimidine and chromene rings are commonly found in nature among heterocyclic compounds^{12,13}. Pyrimidine derivatives, such as thymine, cytosine, and uracil, are essential components of nucleic acids¹⁴. Certain pyrimidine compounds, including veronal and barbituric acid, have hypnotic properties¹⁵. Moreover, pyrrolo [3,2-d] pyrimidine derivatives act as antagonists to adenosine receptor subtypes and enzyme inhibitors. The structural similarity of pyrimidine molecules to flavins contributes to their medicinal significance¹⁶. Pyrimidine fused quinoline derivatives have a wide range of medicinal properties, including antibacterial, antifungal, anticancer, analgesic, antimalarial, antitumor, anti-inflammatory, antiviral, and antioxidant effects¹⁷⁻¹⁹. Also, chromene derivatives have diverse pharmacological properties, such as anticancer²⁰, antimicrobials²¹, antivirals²², anticoagulants²³, and anti-inflammatory activities²⁴. Therefore, it is crucial for the pharmaceutical industry to develop synthetic methods for chromene derivatives. Figure 1 illustrates the structure of some biologically active molecules containing chromene and pyrimidine blocks²⁵. Over the years, a variety of synthetic methods have been developed for pyrimidine or chromene analogs. Among these methods, catalyzed reactions by transition metals are the most attractive approaches for synthesizing chromene and pyrimidine derivatives^{26,27}. Since pyrimidines and chromenes have numerous applications, developing new and efficient routes for synthesizing pyrimidine-fused chromene derivatives has remained a crucial area of research. The fusion of pyrimidines and

Department of Chemistry, Faculty of Sciences, University of Birjand, Birjand 97175-615, Iran. ✉email: gbagherzade@gmail.com

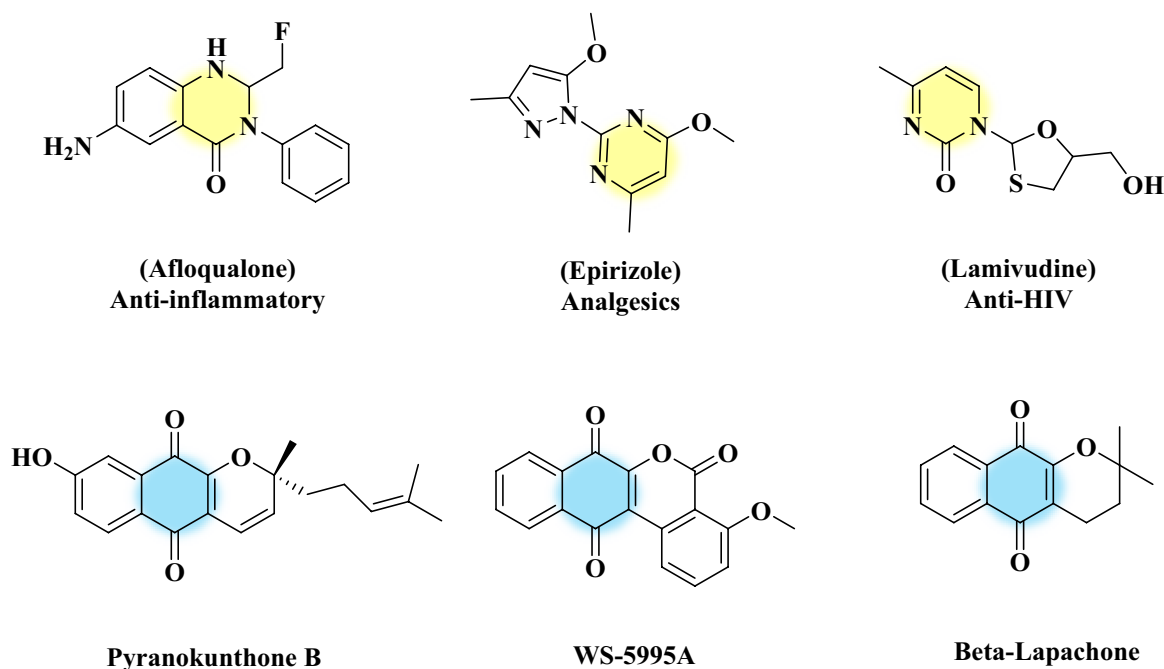


Figure 1. Structures of some biologically active pyrimidine and chromene molecules.

chromenes enhances their biological properties, and chromopyrimidines are used in a range of drugs, including antiplatelets and antithyroid drugs^{28,29}.

Multiplex-modified catalysts have been utilized for the synthesis of chromopyrimidines and their derivatives. However, several reports have highlighted issues such as long reaction times, labor-intensive processes, the use of non-recyclable catalysts, and low product yields^{30–32}. Also, chromopyrimidines can be synthesized from alcohols through multicomponent TOP (tandem oxidation process) reactions^{33,34}. Tandem reactions have attracted considerable attention due to their ability to combine several reactions in a vessel, reducing waste production, and eliminating intermediate separations. Among organic reactions, alcohols are considered environmentally safe chemicals due to their wide accessibility, low cost, availability from renewable biomass sources, low toxicity, and ease of use, storage, transport, and dissolution^{35,36}. The concept of TOP was pioneered by Robert Ireland during his attempts to synthesize poly-ether ionosphere antibiotics³⁷. However, the challenge of separating large quantities of aldehydes produced during the process was addressed by oxidizing alcohols with the Swern reagent and introducing the Wittig reagent to the in situ generated aldehydes³⁸. Since its discovery, TOP has been employed in the synthesis of a wide range of useful materials from alcohols. In recent years, various oxidizing and nucleophilic compounds have been employed in TOP reactions^{39,40}. Further, TOP has been extended to include multicomponent reactions (MCRs), enabling the synthesis of diverse valuable compounds^{41–43}. These processes provide a high atom economy, reducing the need for time-consuming, expensive, waste-generating operations, and purification processes in chemical synthesis⁴⁴. Most recently, multifunctional catalysts have been developed by combining different types of active sites on catalysts for use in tandem catalysis processes. A new area of research focuses on the application of multifunctional catalytic systems in multicomponent TOPs starting from alcohols^{45,46}.

Material or sustainable chemistry focuses on the development of safe materials with catalytic properties^{47–49}. Catalysts play a crucial role in lowering the activation energy and increasing the rate of chemical reactions^{50,51}. Green chemistry emphasizes the reusability and sustainability of catalytic materials, highlighting the need for environmentally friendly, sustainable, and economically effective catalytic systems. Carbon, being abundantly available in nature, has garnered significant attention in research worldwide for its potential as a green catalyst. When designing a catalyst and selecting the appropriate substrate, all aspects of the catalyst's design must be considered, including non-toxicity, biodegradability, environmental friendliness, renewability, abundance, as well as the surface area and morphological attributes of the material^{52–54}.

In this context, chitosan (CS) is recognized as an ideal material with remarkable properties. It possesses active functional groups (hydroxyl: -OH, amino: -NH₂), exhibits non-toxic, high oxidation stability, a large surface area, exceptional physical strength, excellent electron conductivity, and good chemical integrity^{55,56}. However, CS does have certain drawbacks, including solubility in dilute acids, easy aggregation, and poor mechanical strength. Therefore, improving the development of mechanical properties, surface area, and chemical stability of CS is of great importance⁵⁷. Various conventional techniques have been employed to enhance the properties of CS, such as grafting, cross-linking, and composting. Among them, cross-linking reactions of CS are one of the most suitable chemical modification techniques that can enhance the chemical stability, absorption ability, mechanical strength, solubility in acidic environment, and hydrophobicity of CS^{58,59}. So far, various applications of chitosan have been reported, including the removal of radioactive elements, wastewater treatment, catalyst, medicine, fabric production, food, cosmetics, agriculture, biotechnology, nutrition and photography^{60–65}.

Recently, chitosan-based catalysts in water environments with fast recycling capabilities have gained attention from both environmental and economic perspectives⁶⁶. Water, due to its green credentials such as high specific heat capacity, high polarity, a network of hydrogen bonds, high surface tension, high cohesive energy, low cost, and easy accessibility, has emerged as a potential solvent for organic reactions in recent years^{67, 68}.

Eco-friendliness in chemical processes often refers to the use of sustainable and environmentally benign methods. Ionic liquids, known as molten salts, are a fascinating class of chemical compounds consisting of organic cations and organic or inorganic anions. However, they possess distinct properties that set them apart from traditional ionic salts⁶⁹. The unique characteristics of ionic liquids heavily rely on the choice of cations and anions. By selecting different combinations of cations and anions, a wide range of applications for ionic liquids can be achieved. When it comes to Ionic liquids (ILs), they have gained attention as potential alternatives to traditional organic solvents due to their unique properties, such as low volatility, high thermal stability, tunable physicochemical properties, and low vapor pressure^{70, 71}. For this reason, they have been used as green solvents in most organic reactions, including hydrogenation, oxidation, coupling reactions, Diels–alder reaction, etc⁷². However, their high cost and high viscosity have limited their application in organic reactions, as only a thin layer known as the diffusion layer effectively participates in the reaction process. To overcome this limitation, nanocatalysts containing ionic groups have been introduced to address concerns regarding immobilization and recoverability associated with ILs^{73, 74}. This approach enhances the "ionophilicity" of the reagent in the reaction media, facilitating the exchange of counter ions with the leaving group of the reagents^{75, 76}. Additionally, metal complexes bearing an imidazolium moiety can serve as bases and minimize metal leaching in the reaction media. Several comprehensive reviews and articles have emphasized the usefulness of catalytic metal ionic liquids in organic synthesis. These ILs have been successfully employed as recyclable nanocatalysts, offering green and efficient solutions for a wide range of organic transformations. Significant contributions have been made in various areas, including CO₂ conversion, biodiesel formation, coupling reactions, condensation reactions, acetylation, esterification, and multi-component reactions⁷⁷. Over time, numerous biologically significant molecules have been extensively synthesized using catalytic ILs through multi-component reactions including chromenes⁷⁸, 1,2,3-triazoles⁷⁹, dihydropyrano[2,3-*c*]coumarin⁸⁰, 2H-indazolo[2,1-*b*] phthalazine-trione⁸¹, α -amino-phosphonates⁸², furan⁸³, pyrano[2,3-*d*]pyrimidinone⁸⁴, xanthenes⁸⁵, Diels–Alder reaction⁸⁶ and etc^{87, 88}.

Finally, given the wide range of applications of chitosan in various industries, it has been utilized as a catalyst in multicomponent reactions. Previous research has shown that the oxidation of alcohols to aldehydes is a highly selective and controllable reaction. However, there are no existing reports on the synthesis of chromopyrimidine derivatives from alcohols or the symmetrical synthesis of these compounds using bis-aldehyde derivatives. Therefore, we have developed an efficient and cost-effective one-pot tandem method for the synthesis of chromopyrimidine derivatives using readily available substrates and catalysts. In this study, we synthesized a recyclable cobalt/copper heterogeneous bimetallic nanohybrid from chitosan (Fig. 2: mTEG-CS-Co/Cu-Schiff-base/IL) that exhibited excellent performance in the tandem oxidation-condensation reaction of chromopyrimidine from alcohols. The cooperative, and synergistic effects in mTEG-CS-Co/Cu-Schiff-base/IL were investigated through various control experiments (Fig. 2).

Experimental

All the specifications of chemicals and devices used are available in the support information file.

Preparation of the CS-Schiff-base/IL

The synthesis of the chitosan was performed according to an already-established procedure⁸⁹. Firstly, purified CS (1000 mg) was dissolved in 80 mL of a diluted 1% (w/w) aqueous AcOH solution at room temperature for 12 h. In another round bottom flask, 0.016 mol of 5-(chloromethyl)-2-hydroxybenzaldehyde^{90–92} was dissolved in CH₂Cl₂. Then, the aldehyde solution was added dropwise to the CS solution under stirring and the mixture was heated to 50 °C for 5 h. After the end of the reaction, 0.016 mol of 1-Methyl imidazole was added to the CS-Schiff-base solution, and the mixture was refluxed for 24 h. Finally, the reaction mixture was collected by centrifugation, and washed with CH₂Cl₂ (3 × 10 mL) to remove any unreacted imidazole, and aldehyde and dried in a vacuum oven at 40 °C for 12 h.

Preparation of the mTEG-CS-Schiff-base/IL

In this method, the mTEG-CS-Schiff-base/IL is prepared by stirring a mixture of mTEG (tosylate mono-methoxy triethylene glycol: 20 mmol), (1 g), and K₂CO₃ (20 mmol) in dry acetonitrile (50 mL) at 60 °C for 24 h. The resulting solid material is separated by centrifugation, washed with water and ethanol (3 × 10 mL), and then dried in an oven at 50 °C for 24 h.

Preparation of the mTEG-CS-Co/Cu-Schiff-base/IL nanohybrid

Finally, the mTEG-CS-Co/Cu-Schiff-base/IL nanohybrid is prepared by adding CoCl₂ (2 mmol) and CuCl₂ (2 mmol) to the mixture of mTEG-CS-Schiff-base/IL (1 g) in EtOH (20 mL) and stirring at 80 °C for 24 h. After the reaction, the mixture is cooled, filtered off, washed with ethanol (2 × 20 mL), and dried in an oven at 60 °C for 24 h. The amount of Co and Cu loading on the nanohybrid is measured using Atomic Absorption Spectroscopy (AAS) and Inductively Coupled Plasma (ICP) instruments to obtain certainty about the results. The results from both analyses show a small difference of 0.006 between them. The analysis shows that the amount of copper and cobalt in one gram of the catalyst is 0.60 mmol and 0.52 mmol, respectively, and the percentage of the metals is 6.8%w and 6.3%w for Cu and Co, respectively. For comparison, the monometallic copper and cobalt catalysts synthesized separately have metal loadings of 7.9% w/w for Cu and 7.4% w/w for Co in one gram of catalyst, respectively.

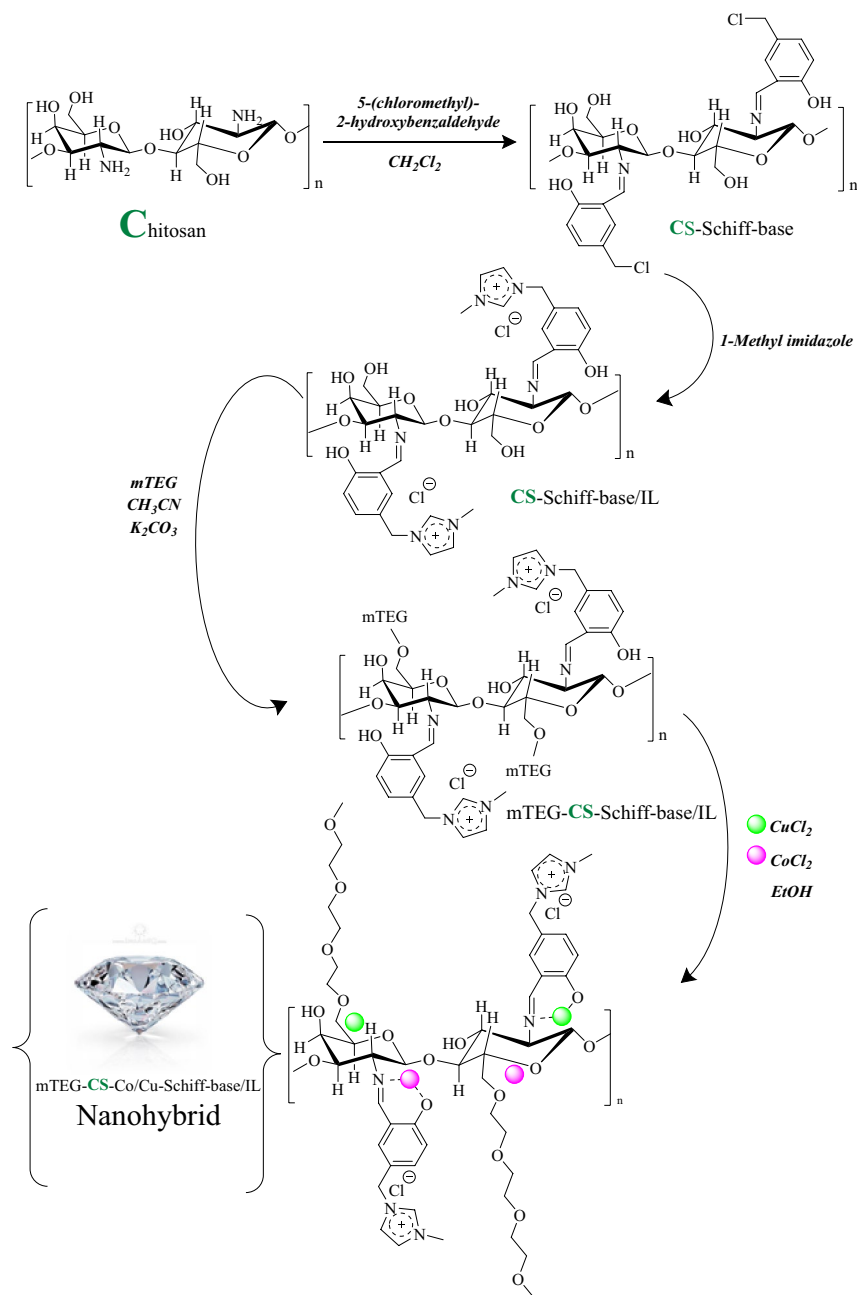


Figure 2. Schematic illustration of mTEG-CS-Co/Cu-Schiff-base/IL nanohybrid synthesis strategy.

General procedure for the tandem one-pot preparation of chromenopyrimidine-2,5-dione reaction with alcohol

A mixture of alcohol (1.2 mmol), urea (1 mmol), and 4-hydroxycoumarin (1 mmol) in the presence of the nanohybrid (3 mg) was stirred in H_2O (5 ml) at the appropriate time and temperature. The progress of the reaction was checked by TLC. Once the desired reaction is complete, the catalyst is removed, and the product is allowed to precipitate. Finally, the products were purified by recrystallization from EtOH (See spectral data in SI File).

General procedure for the chromenopyrimidine-2,5-dione and thioxochromeno pyrimidin-5-one reactions with Bis-aldehyde

The synthesis of bis-aldehyde derivatives was conducted following an established procedure^{93,94}. The one-pot synthesis of Chromenopyrimidine-2,5-dione was carried out in a round-bottom flask using bis-aldehyde (1 mmol), urea (2 mmol), and 4-hydroxycoumarin (2 mmol) in the presence of mTEG-CS-Co/Cu-Schiff-base/IL nanohybrid (4 mg), under aerobic conditions in H_2O at 50 °C. The progress of the reaction was monitored using TLC. Finally, the products were purified by recrystallization from EtOH (See spectral data in SI File).

Result and discussion

Nanohybrid was synthesized as predestined in Fig. 2. Initially, 5-(chloromethyl)-2-hydroxybenzaldehyde is coated with chitosan to obtain CS-Schiff-base. The CS-Schiff-base/IL is then formed by reacting the chlorine groups on the Schiff base chains with methyl imidazole. To introduce a phase transfer functional group, monomethoxy triethylene glycol (mTEG) is added to the hydroxyl group of the CS-Schiff-base/IL. This addition enhances the solubility and stability of the nanohybrid. Finally, cobalt and copper nanoparticles are immobilized on mTEG-CS-Co/Cu-Schiff-base/IL by adsorption of CoCl_2 and CuCl_2 on the nanohybrid. The synthesized catalyst was characterized using various techniques including XRD, FE-SEM, TEM, TGA, EDX-EDS, FT-IR, AFM, and ICP.

FT-IR spectra are one of the best instruments to provide adequate data to clarify the bonding of the synthesized compounds. Figure 3 shows the FT-IR spectra of pure chitosan, CS-Schiff-base/IL and mTEG-CS-Co/Cu-Schiff-base/IL nanohybrid. In Fig. 3a (CS), a strong peak is observed in the FT-IR spectra of chitosan in the region range of 3000 and 3600 cm^{-1} , corresponding to the stretching vibrations of amine and hydroxyl groups. The bands observed at 2876, 1643, 1074, and 1022 cm^{-1} can be attributed to the C-H aliphatic, N-H bending, C-N, and C-O stretching, respectively. In the spectrum of CS-Schiff-base/IL (Fig. 3b), the absorption bands around 3101, 1690, 1500–1598, and 753 cm^{-1} are assigned to the stretching vibration of C-H aromatic ring, C=N Schiff base/imidazole, C=C aromatic/imidazole ring, and C-Cl stretch bonds. Comparing the mTEG-CS-Co/Cu-Schiff-base/IL spectrum with the CS-Schiff-base/IL spectrum, it is evident that most of the characteristic peaks are stronger in the former spectrum. This enhancement is attributed to the addition of the mTEG chain and Co/Cu metal ions. However, mTEG-CS-Co/Cu-Schiff-base/IL spectrum indicates the formation of nanohybrid groups (Fig. 3c). Notably, compared to CS and CS-Schiff-base/IL, the mTEG-CS-Co/Cu-Schiff-base/IL spectrum exhibits multiple new bands at 463, 461, 542, and 625 cm^{-1} , corresponding to Cu-N, Co-N, Cu-O, and Co-O groups, respectively. These bands indicate the successful stabilization of metallic groups⁹⁵. Furthermore, the FT-IR spectrum of the mTEG-CS-Co/Cu-Schiff-base/IL nanohybrid demonstrates a shift (13 cm^{-1}) in the stretching vibration of C=N groups to lower wavenumbers. This shift confirms the coordination of Co(II) and Cu(II) metal ions with the nitrogen and oxygen atoms of the Schiff base.

Figure 4 shows that the nanosized mTEG-CS-Co/Cu-Schiff-base/IL nanohybrid exhibits no evidence of aggregation, and all particles are nearly spherical in shape. The largest particle size observed in the sample is 28 nm, which is found in the embedded mTEG-CS-Co/Cu-Schiff-base/IL nanohybrid.

Based on the Energy Dispersive X-Ray (EDX) analysis depicted in Fig. 5, it is evident that the nanohybrid can be successfully functionalized to serve as a catalyst. The EDX spectrum shows the presence of various elements in the nanohybrid, that the weight percentages of these elements in the nanohybrid are as follows: 51.2% for C, 17.5% for O, 5.2% for N, 12.4% for Cu, 11.5% for Co, and 2.1% for Cl. Furthermore, the EDS spectrum of the nanohybrid confirms its full chemical complexity, indicating that the nanocomposite comprises a combination of these elements in a chemically integrated manner.

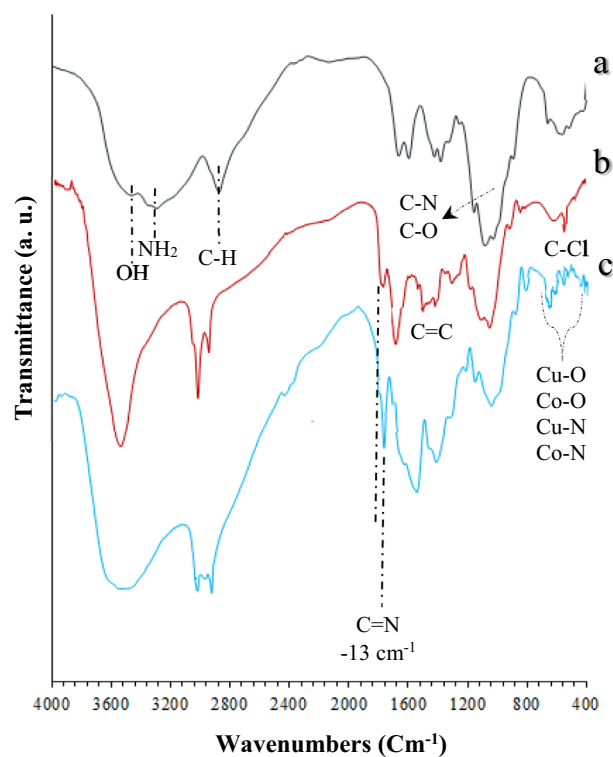


Figure 3. FT-IR spectra of (a) Chitosan, (b) CS-Schiff-base/IL and (c) mTEG-CS-Co/Cu-Schiff-base/IL nanohybrid.

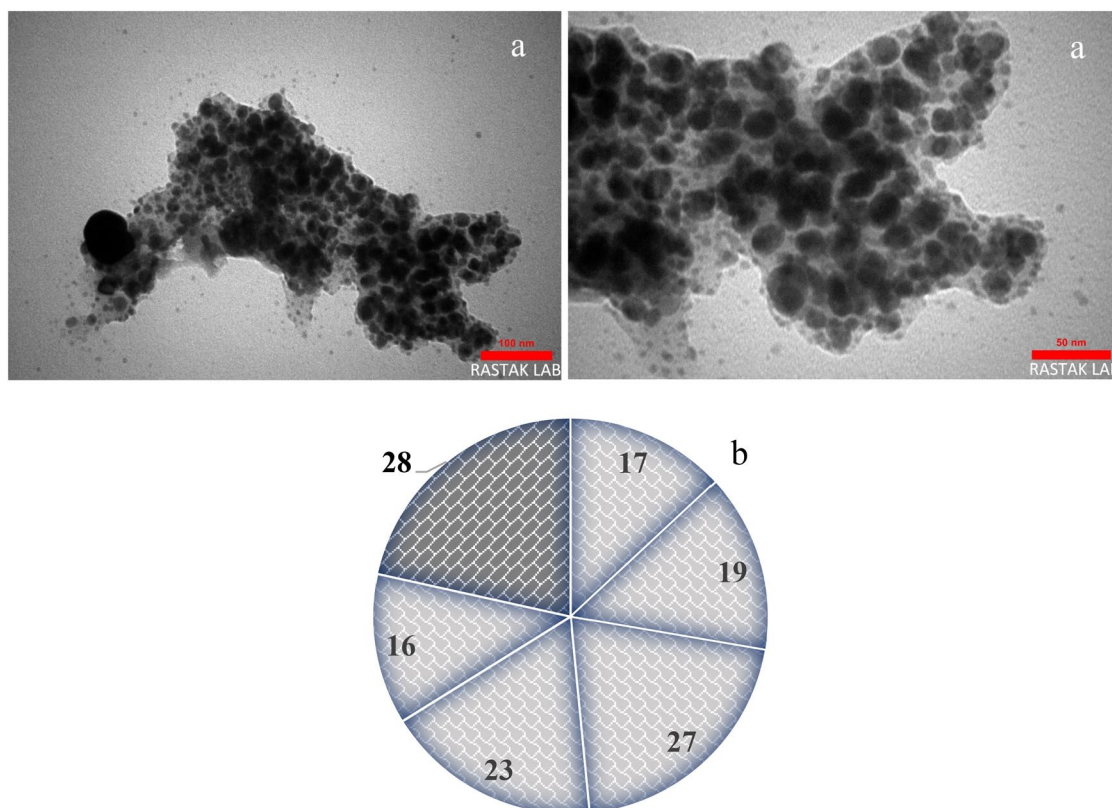


Figure 4. TEM image (a) and Particle size distribution histogram (b) of mTEG-CS-Co/Cu-Schiff-base/IL nano hybrid.

The surface morphologies of the nano hybrid were visualized directly using FE-SEM (Fig. 6). As shown in Fig. 6, the roughness illustrated on the surface of the nano hybrid indicates chemical modification of the chitosan surface.

In Fig. 7, the TGA data from mTEG-CS-Schiff-base/IL and nano hybrid indicate three and two weight loss steps, respectively. The first weight loss step occurs in the temperature range of 25–170 °C and is attributed to the evaporation of adsorbed water molecules (15% for mTEG-CS-Schiff-base/IL and 1.5% for nano hybrid). In the second stage, a total weight loss of 50% for mTEG-CS-Schiff-base/IL and 4.8% for the nano hybrid is observed. This weight loss is associated with the decomposition of the Schiff-base units and the chitosan chains as a polysaccharide.

As illustrated in Fig. 8, XRD patterns for mTEG-CS-Schiff-base/IL and nano hybrid are displayed. The chitosan monomer structure contains strong intermolecular hydrogen bonds. In the XRD pattern of mTEG-CS-Schiff-base/IL, two characteristic peaks in the range of $2\theta = 10^\circ\text{--}20^\circ$ indicate its semi-crystalline nature (Fig. 8a). However, the XRD pattern of the nano hybrid (Fig. 8b) displays a range of peaks varying from small to intense. The broad peak observed at $10^\circ\text{--}20^\circ$ in the XRD pattern of the mTEG-CS-Co/Cu-Schiff-base/IL nano hybrid corresponds to the amorphous nature of chitosan. Additionally, there are diffraction peaks attributed to cobalt (two weak sharp peaks) and copper (three weak to moderate peaks) observed at 17.20° , 19.05° and 42.35° , 51.70° , 74.05° , respectively^{96,97}. These peaks indicate the crystalline changes resulting from the coordination of metals with the modified chitosan polymer. Moreover, the deformation of hydrogen bonds during condensation leads to a decrease in the crystallinity of chitosan.

Real-time visualization of the nano hybrid is possible through in situ atomic force microscopy (AFM). Figure 9 illustrates the topographical structure of thin films from AFM images. Different parameters, such as root mean square roughness (RMS), can be utilized to quantify the topographical characteristics of a surface. The RMS roughness of an mTEG-CS-Co/Cu-Schiff-base/IL nano hybrid thin film was measured to be 26.64 nm. In the 3D image, multiple peaks representing the porous and uneven surface of the nano hybrid are evident. This suggests that the modification of the chitosan surface leads to an increase in number of pores and surface roughness.

The catalytic activity of the mTEG-CS-Co/Cu-Schiff-base/IL nano hybrid in the synthesis of chromenopyrimidine via *multicomponent TOP*

After successfully synthesizing and identifying mTEG-CS-Co/Cu-Schiff-base/IL nano hybrid, its catalytic performance was probed in the chromenopyrimidine-2,5-dione reaction. The optimization of reaction parameters was studied by the multi component reaction between benzyl alcohol, 4-hydroxycumarine, and urea as a model reaction. First, the model reaction was carried out in the absence of nano hybrid and in the presence of water as a solvent under reflux conditions. Without the nano hybrid, only trace amounts of the desired product were

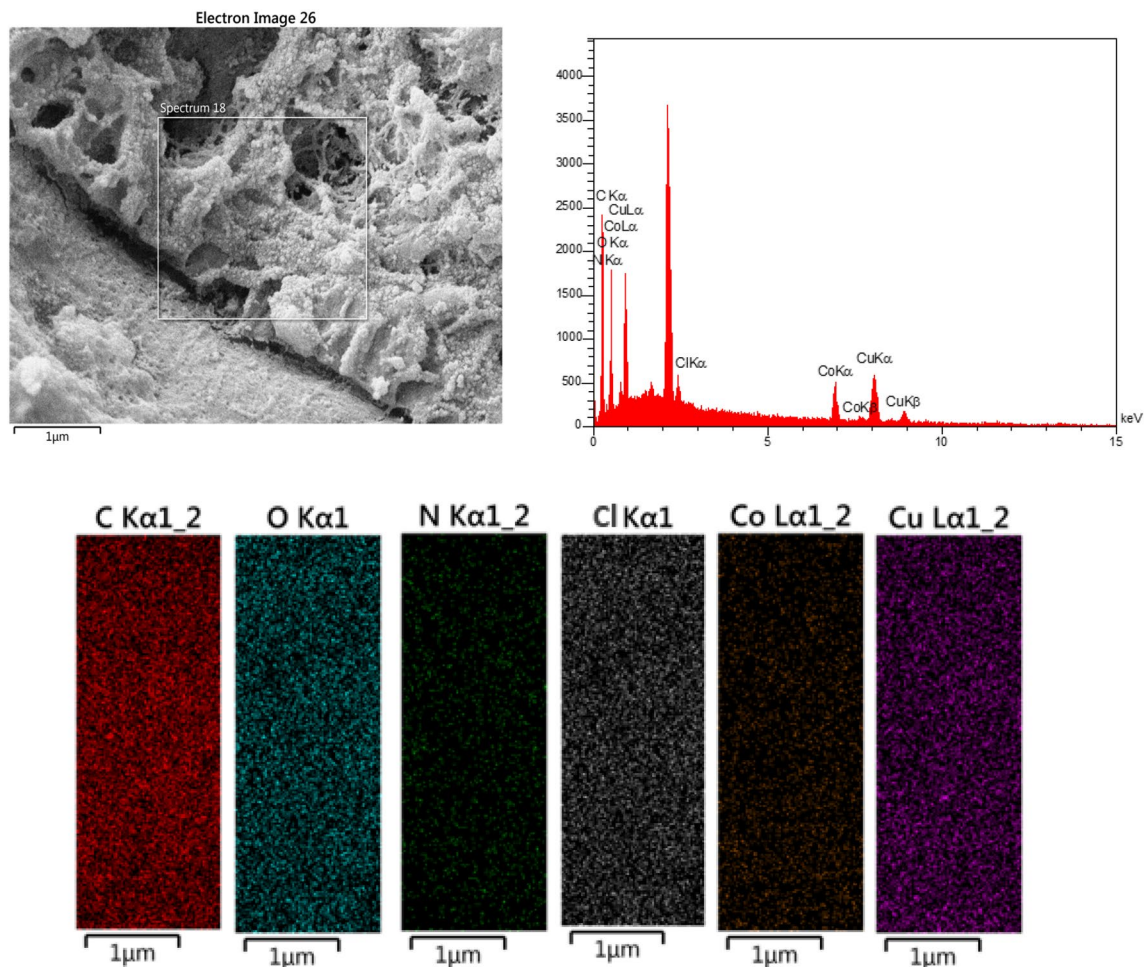


Figure 5. EDX-EDS spectra and elemental mapping of mTEG-CS-Co/Cu-Schiff-base/IL nanohybrid.

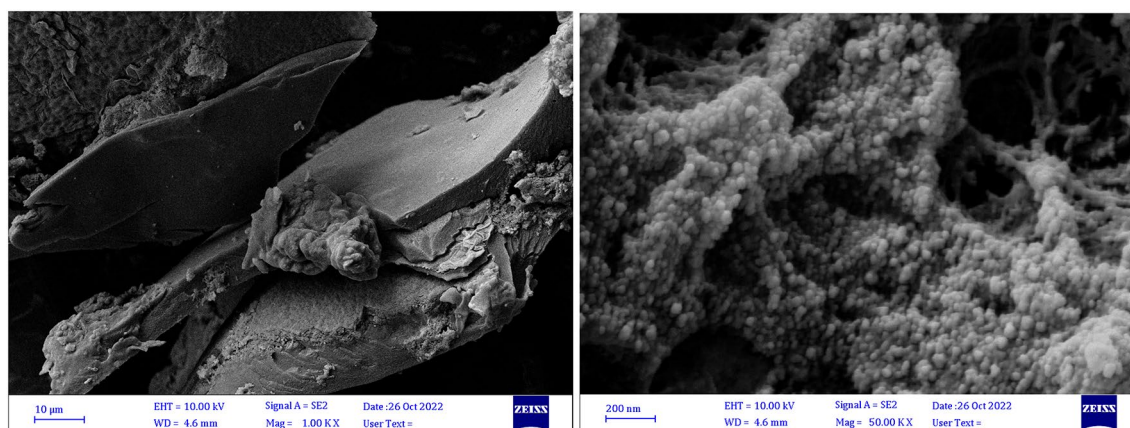


Figure 6. FE-SEM images of mTEG-CS-Co/Cu-Schiff-base/IL nanohybrid.

observed, demonstrating the importance of the catalyst in promoting the reaction. However, before investigating the chromenopyrimidine-2,5-dione reaction, benzyl alcohol was used as a model compound to investigate the oxidation activity of the catalyst. The influence of solvent, catalyst amount, diverse oxidants, and temperature on the oxidation of benzyl alcohol to benzaldehyde was investigated (Fig. 10). First, as can be seen in Fig. 10a, a range of solvents including water, dichloromethane, ethanol, ethyl acetate, acetonitrile and a solvent-free reaction was investigated. Among the solvents investigated, water emerged as the preferred solvent for this reaction. Through experimentation and data analysis, it was observed that ethyl acetate, dichloromethane, and acetonitrile exhibited lower improvement in efficiency compared to water, in the oxidation reaction of alcohol. The low efficiency of solvents in this reaction may be attributed to their lower solubility, unintended interferences, and unfavorable

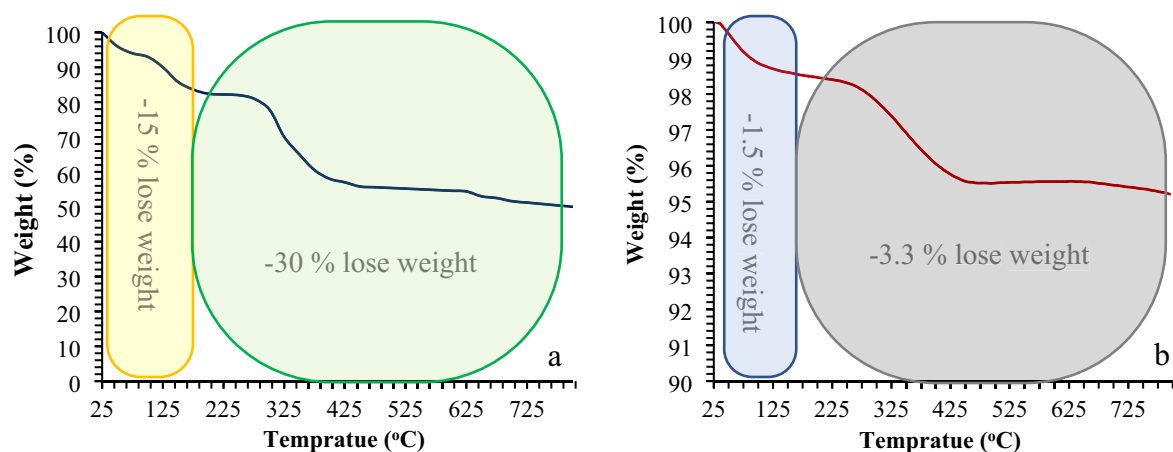


Figure 7. TGA weight-loss curve for the mTEG-CS-Schiff-base/IL (a) and mTEG-CS-Co/Cu-Schiff-base/IL (b) nano hybrid.

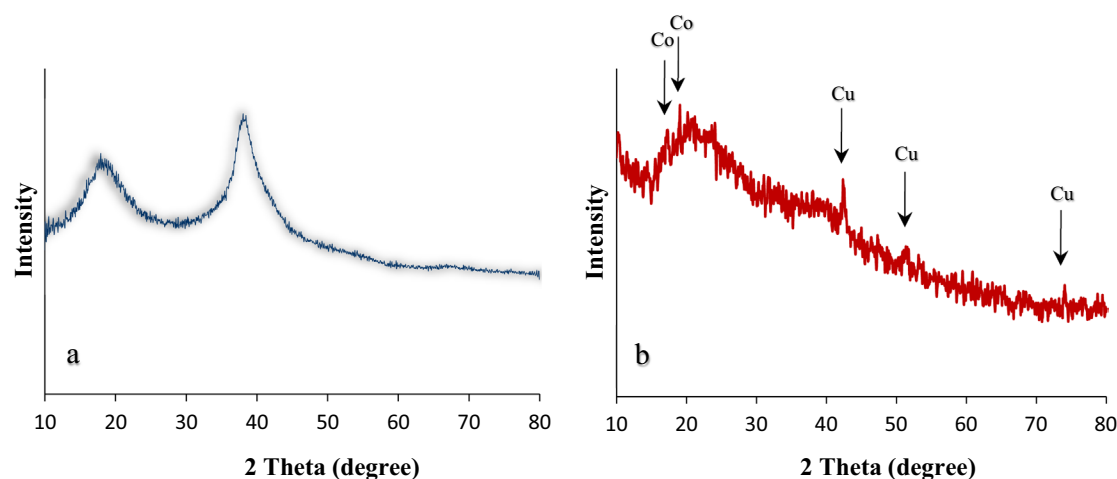


Figure 8. XRD patterns of mTEG-CS-Schiff-base/IL (a) and mTEG-CS-Co/Cu-Schiff-base/IL nano hybrid (b).

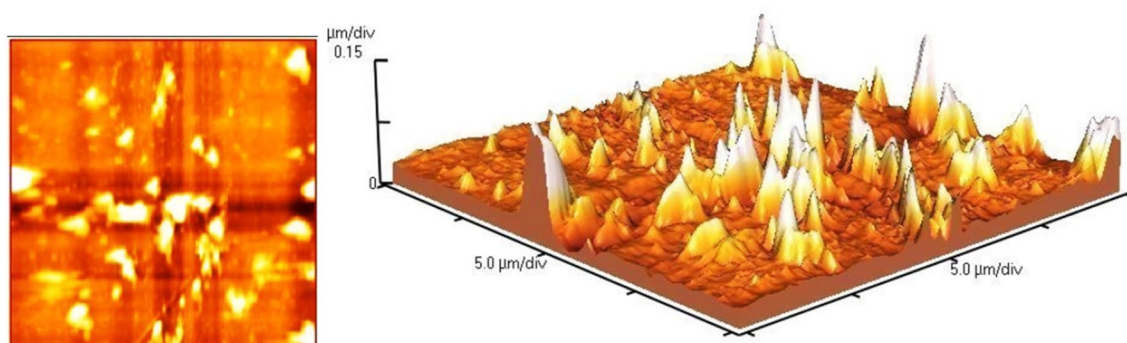


Figure 9. AFM images of mTEG-CS-Co/Cu-Schiff-base/IL nano hybrid.

physical and chemical properties. Next, the effect of reaction temperature was examined in the oxidation reaction of alcohol (Fig. 10b). The temperature range investigated was between 25 to 60 °C, and it was found that a temperature of room temperature (25 °C) yielded better results compared to higher temperatures. One reason for the decrease in efficiency at higher temperatures can be attributed to the increase in reaction rate. As the temperature rises, the reaction rate also increases. This can lead to the formation of byproducts or impurities that can decrease the overall efficiency. Therefore, to improve efficiency, the optimal temperature for this reaction could be room temperature. In the following, the oxidation reaction of alcohol (Fig. 10c) was investigated using varying

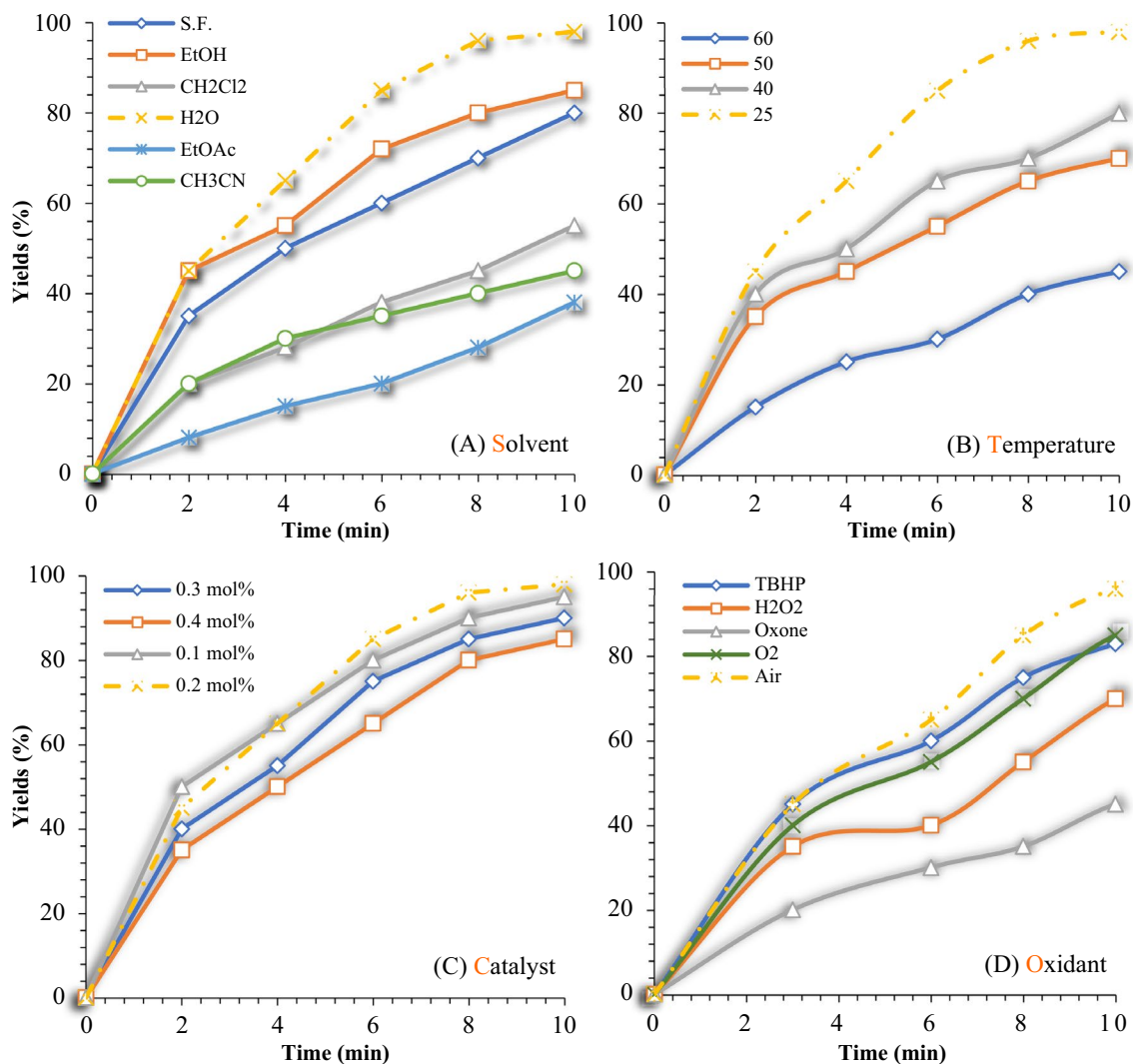



Figure 10. The screening effect of the solvent (a), temperature (b), amount catalyst (c), and oxidant (d) on the oxidation of alcohols reaction. Oxidation of alcohols reaction conditions: Benzyl alcohol (1 mmol), mTEG-CS-Co/Cu-Schiff-base/IL (0.2 mol%), H₂O, R.T, open air.

amounts of mTEG-CS-Co/Cu-Schiff-base/IL nano hybrid. Among the different catalyst concentrations tested, it was found that 0.2 mol% of the catalyst yielded the best results. Further increasing or decreasing the catalyst concentration did not significantly improve the yield. Higher catalyst concentrations may saturate the reaction system, leading to overcrowding of active sites and reduced efficiency. Conversely, lower catalyst concentrations may not provide enough active sites for effective catalysis, resulting in lower yields. Therefore, 0.2 mol% of the catalyst appears to strike the right balance, maximizing the yield in the oxidation reaction of alcohol. Finally, the role of oxidants in oxidation reactions is crucial, and in order to identify the most effective oxidant, different strong and weak oxidants were evaluated under the same reaction conditions (Fig. 10d). Among the oxidants tested (O₂, H₂O₂, Air, TBHP, and Oxone), aerobic conditions played a significant role in conversion and selectivity. This suggests that atmospheric oxygen present in the air serves as an efficient oxidizing agent for the oxidation reaction of interest. The preference for air as the oxidant could be attributed to its availability, cost-effectiveness, and compatibility with the reaction system. The use of other oxidants, either strong or weak, did not yield as favorable results. The presence of a strong oxidant in the alcohol oxidation reaction led to a decrease in efficiency. The strong oxidant can compete with the catalyst and extract active species from it, resulting in reduced catalyst activity and overall reaction efficiency. Also, the strong oxidant can generate undesired side products, which can negatively impact the overall yield. Furthermore, it can interfere with electron transfer processes by absorbing electrons from the catalyst, disrupting the electron transfer pathway and leading to decreased reaction efficiency. Lastly, the presence of a strong oxidant can cause damage and alteration to the catalyst, further diminishing its catalytic activity and reducing the overall reaction efficiency.

Under optimal reaction conditions, a variety of primary benzylic alcohols were oxidized to assess the applicability of the protocol (R.T in H₂O under aerobic conditions). Electron-withdrawing and higher steric hindrance increased reaction times for benzylic alcohols (Table 1, entries 2, 4, 6, 7, 9). The results showed no significant



Entry	Substrate (R)	Product	Time (min)	Yield ^a (%)
1	H	Benzaldehyde	10	98
2	2-Cl	2-Chlorobenzaldehyde	10	93
3	4-Cl	4-Chlorobenzaldehyde	10	90
4	2-Br	2-Bromobenzaldehyde	15	87
5	4-Br	4-Bromobenzaldehyde	25	83
6	2-NO ₂	2-Nitrobenzaldehyde	30	87
7	4-NO ₂	4-Nitrobenzaldehyde	30	90
8	4-MeO	2-Methoxybenzaldehyde	20	95
9	2-OH	2-Hydroxybenzaldehyde	20	85
10	4-CH ₂ OH	Terephthalaldehyde	45	80

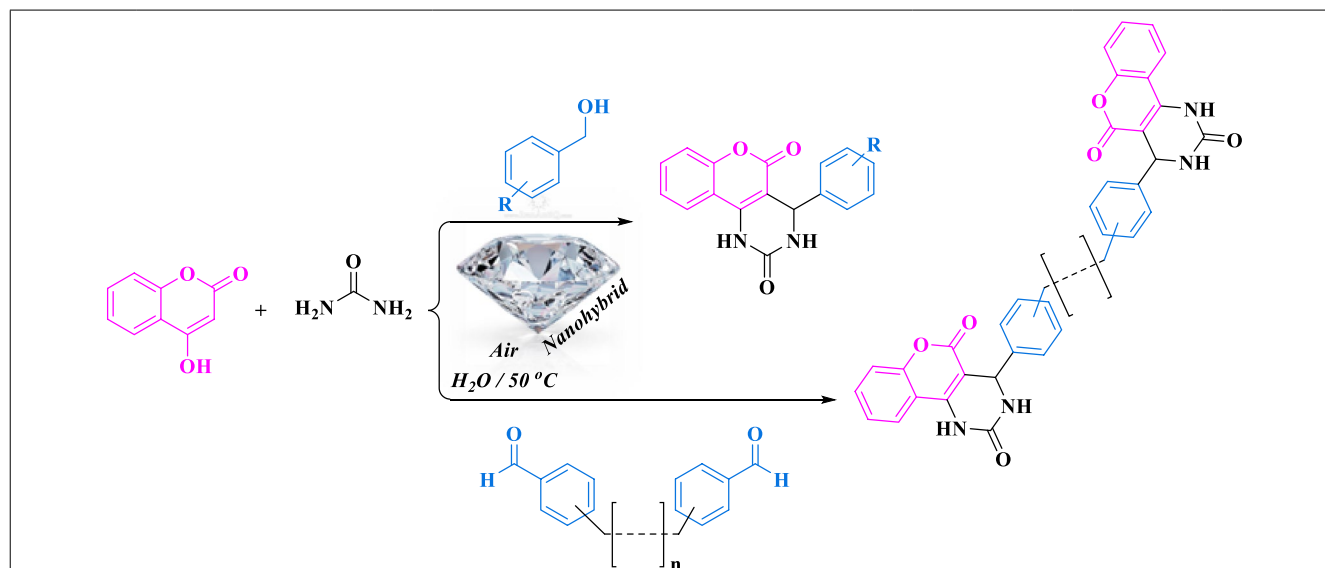
Table 1. Oxidation of benzyl alcohols to corresponding aldehydes in the present of mTEG-CS-Co/Cu-Schiff-base/IL nanohybrid. Reaction conditions: benzyl alcohol derivatives (1 mmol), mTEG-CS-Co/Cu-Schiff-base/IL (0.2 mol%), H₂O, R.T, open Air. ^aIsolated product yields.

difference in the efficiency of alcohols bearing electron-withdrawing and electron-donating groups, with excellent efficiency for all derivatives, without excessive oxidation to carboxylic acid or ester.

Following the successful oxidation of alcohols, we investigated the effectiveness of the catalyst mTEG-CS-Co/Cu-Schiff-base/IL in the synthesis of chromenopyrimidine via a multicomponent tandem oxidation process. The chromenopyrimidine derivatives were synthesized using the nanohybrid under optimized conditions, involving the reaction of alcohols or bis-aldehydes with 4-hydroxycoumarin and urea, resulting in yields of 85–98% (as shown in Table 2). It can be inferred from Table 2 that the product yields of benzyl alcohols with electron-withdrawing groups are higher compared to those with electron-donating groups. Importantly, the reactions proceeded smoothly without generating any side products, particularly oxidation products. These observations highlight the remarkable catalytic activity and selectivity of the catalyst for synthesis of chromenopyrimidines from alcohols and bis-aldehydes with 4-hydroxycoumarin and urea. Moreover, the application of this nanohybrid was evaluated for the synthesis of bis-aldehyde derivatives (as shown in Table 2), resulting in good to high yields.

To further understand the individual contributions of the components in the nanohybrid for the tandem aerobic oxidative reactions, separate control experiments were conducted for the model one-pot chromenopyrimidine reaction under the same conditions. The repeatability of the reactions, assessed by averaging the results of 4 experiments performed under identical conditions (Table 3). As shown in Table 3, the bare chitosan showed no efficiency (Table 3, entry 1). CS-Schiff-base/IL and mTEG-CS-Schiff-base/IL showed limited oxidation activity under open-air conditions, resulting in only trace amount of chromenopyrimidine was synthesized with them after 2 h (Table 3, entries 2, 3). Among the nanohybrid components, the performance of mTEG-CS-Co-Schiff-base/IL and mTEG-CS-Cu-Schiff-base/IL was valuable and significant due to the presence of copper and cobalt metals (Table 3, entries 4, 5). According to the ICP analysis, copper was found to be loaded in higher amounts than cobalt. Therefore, the mTEG-CS-Cu-Schiff-base/IL nanohybrid exhibited higher efficiency in alcohol oxidation and chromenopyrimidine (Table 3, entry 5). Interestingly, the most remarkable results were obtained using the bimetallic system mTEG-CS-Co/Cu-Schiff-base/IL as a catalyst, demonstrating its high performance in the oxidation step and confirming the synergistic effect of cobalt and copper centers in the nanohybrid for the green one-pot reaction. The obtained results clearly showed the synergistic effect and cooperative activity between the two metals, cobalt and copper, in the nanohybrid for the tandem oxidation-condensation reaction, achieved within 15 min. The catalyst metals play a crucial role in facilitating the reaction simultaneously. This study highlights that the simultaneous utilization of copper and cobalt catalyst metals in the chromenopyrimidine reaction enhances the catalyst's performance and increases the reaction efficiency, surpassing the performance achievable with each metal alone.

To check the reusability of the nanohybrid, a recycling test was performed for the model reaction (benzyl alcohol, urea, and 4-hydroxycoumarin) under optimized conditions. The presence of the hydrophilic mTEG and imidazole tag in the catalyst facilitated the movement of organic molecules toward the catalyst, promoting faster interactions and reactions. However, the mTEG-CS-Co/Cu-Schiff-base/IL catalyst itself was hydrophobic and remained dispersed in the aqueous phase without any affinity for the organic solution (Fig. 11). Consequently, the catalyst remained in the aqueous phase until the product was extracted using EtOAc. Then, the aqueous phase was recharged with benzyl alcohol, urea, and 4-hydroxycoumarin for the subsequent run without separating the catalyst. As shown in Fig. 11, a slight decrease in catalytic activity of the nanohybrid was observed after the 6th run, with a decrease of only 5%. Furthermore, the amount of copper and cobalt leaching into the solution

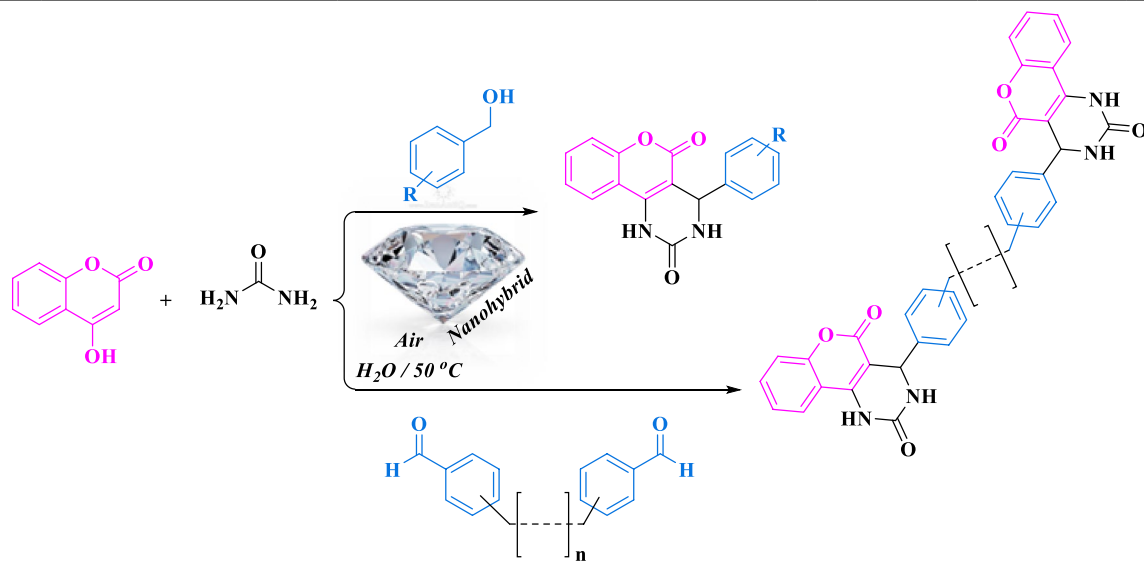


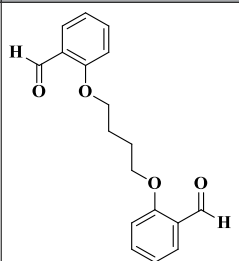
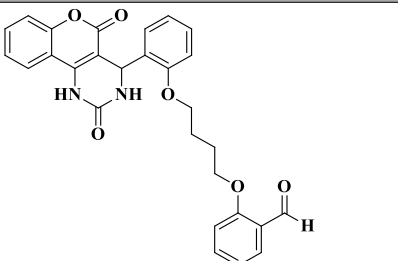
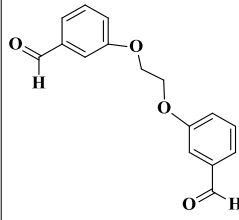
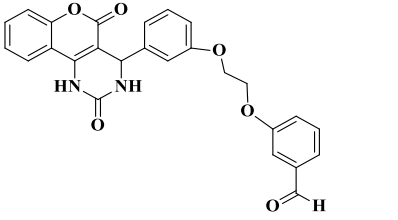
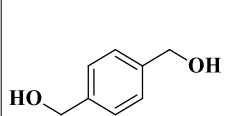
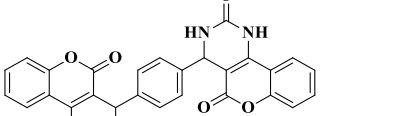
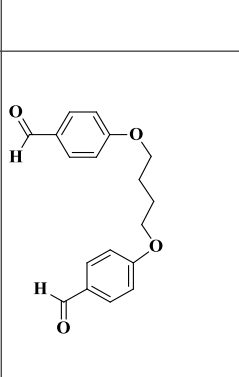
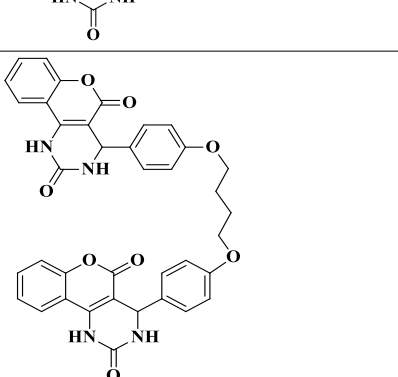
Entry	Benzyl alcohol Bis-aldehyde	Product	Time (min)	Yield ^a (%)	M.P. ($^\circ\text{C}$)
1a			15	98	210–212
2b			15	95	201–203
3c			15	95	259–261
4d			15	92	205–208
5e			10	97	205–207
6f.			15	95	New 205–207
7g			15	95	New 248–250

Continued

Entry	Benzyl alcohol Bis-aldehyde	Product	Time (min)	Yield ^a (%)	M.P. (°C)
8 h			10	95	New 244–245
9i			10	95	New 263–265
10j			20	96	New 225–228
11 k			15	95	New 238–240
12l			15	92	New 223–225

Continued



Entry	Benzyl alcohol Bis-aldehyde	Product	Time (min)	Yield ^a (%)	M.P. (°C)
13 m			20	88	New 222–225
14n			15	90	New 236–238
15o			20	85	New 230–233
16p			20	95	New 244–246

Continued

Entry	Benzyl alcohol Bis-aldehyde	Product	Time (min)	Yield ^a (%)	M.P. (°C)
17q			20	93	New 230–232
18r			20	85	New 235–237
19s			20	90	New 242–244

Table 2. One-pot reaction of benzyl alcohols or bis-aldehydes with 4-hydroxycoumarin and urea catalyzed by mTEG-CS-Co/Cu-Schiff-base/IL. Reaction conditions: Benzyl alcohols or bis-aldehydes (1.2 mmol), 4-hydroxycoumarin (1 or 2 mmol), urea (1 or 2 mmol), mTEG-CS-Co/Cu-Schiff-base/IL (0.2 mol%), H₂O, 50 °C, aerobic condition. ^aIsolated product yields.

during the chromenopyrimidine reaction after the 6th run was measured using ICP analysis of the nanohybrid. The analysis revealed that the weight percentages of copper (Cu) and cobalt (Co) remained unchanged from their corresponding fresh values: Cu 6.5 w%, Co 6.1 w%. These findings indicate that the nanohybrid catalyst exhibited very low leaching rates, which is environmentally significant. On the other hand, to assess the durability and structure of the catalyst, the recovered catalyst was subjected to FT-IR analyze after the 6th run. Figure 1s

Entry	Catalyst	Amount of metal loading per gram (%W)	Oxidation of alcohol ^a temp./time/yield (%)	Chromenopyrimidine ^b temp./time/yield (%)
1	Chitosan	–	70 °C/6 h/–	80 °C/45 min/–
2	CS-Schiff-base/IL	–	70 °C/2 h/Trace	80 °C/45 min/Trace
3	mTEG-CS-Schiff-base/IL	–	70 °C/2 h/Trace	80 °C/45 min/Trace
4	mTEG-CS-Co-Schiff-base/IL	7.4	60 °C/60 min/90	80 °C/90 min/82
5	mTEG-CS-Cu-Schiff-base/IL	7.9	60 °C/45 min/95	80 °C/90 min/90
6	mTEG-CS-Co/Cu-Schiff-base/IL	6.8 (Cu) 6.3 (Co)	R.T/10 min/98	50 °C/15 min/98

Table 3. Control experiments designed for alcohol oxidation and preparation of chromeno pyrimidine reaction in one pot. ^aReaction conditions: Benzyl alcohol derivatives (1 mmol), nano hybrid (0.2 mol%), H₂O, open Air. ^bReaction conditions: Benzyl alcohol (1.2 mmol), 4-hydroxycoumarin (1 mmol), urea (1 mmol), nano hybrid (0.2 mol%), H₂O, aerobic condition.

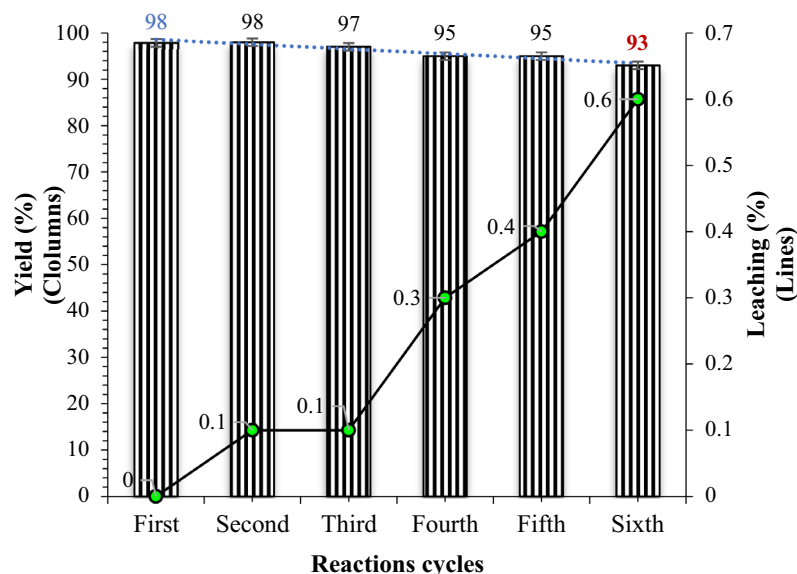


Figure 11. The reusability of catalysts for synthesis of chromeno pyrimidine.

displays the FT-IR analysis results for the recovered catalyst, confirming that the chemical structure of the catalyst remained intact throughout the recycling process (Fig. 1S: See spectral data in SI File).

Finally, to indicate the heterogeneous nature of the catalyst, Hg poisoning tests and hot filtration were conducted on the chromeno pyrimidine synthesis under optimal conditions (Fig. 11). In this method, metallic mercury is used to poison M⁰ clusters or nanoparticles that function as catalytic centers, while it remains inert towards molecular metal complexes. If the addition of metallic mercury inhibits the catalytic reaction, it suggests the involvement of a cluster or nanoparticle in the catalytic mechanism (Fig. 12).

In Fig. 13, the blue cone represents progress of the model reaction in the presence of the mTEG-CS-Co/Cu-Schiff-base/IL as the catalyst in the range of 0–15 min. In the green cone experiment, the catalyst was removed from the reaction mixture through filtration after six minutes, and the reaction was allowed to continue, but no significant progress was observed. In the two separate experiments denoted by the red and yellow cone, the red cone represents the addition of mercury (Hg) from the beginning of the reaction. In this case, the reaction only progressed to 10% completion after 15 min, indicating that the presence of mercury inhibited the catalytic activity of the mTEG-CS-Co/Cu-Schiff-base/IL catalyst. On the other hand, the yellow cone represents the addition of mercury to the reaction vessel after six minutes. In this scenario, the reaction did not progress significantly, suggesting that the addition of mercury at this point did not significantly affect the already initiated catalytic process. These observations indicate that the presence of mercury has a negative impact on the catalytic activity of the mTEG-CS-Co/Cu-Schiff-base/IL catalyst.

Table 4 presents a comparison of the nano hybrid catalyst with various other catalysts previously employed in the same reaction. The results demonstrate that our designed catalyst exhibits efficient catalytic activity compared to the other catalysts tested. The reaction proceeds to completion with the appropriate amount of mTEG-CS-Co/Cu-Schiff-base/IL catalyst, and it provides the desired products from alcohol derivatives in a short period of time. It was found that these monometallic catalysts possess a certain degree of catalytic activity on their own. Furthermore, the catalytic performance of mTEG-CS-Co-Schiff-base/IL and mTEG-CS-Cu-Schiff-base/IL as monometallic catalysts was also investigated. However, when comparing the catalytic activity of the nano hybrid

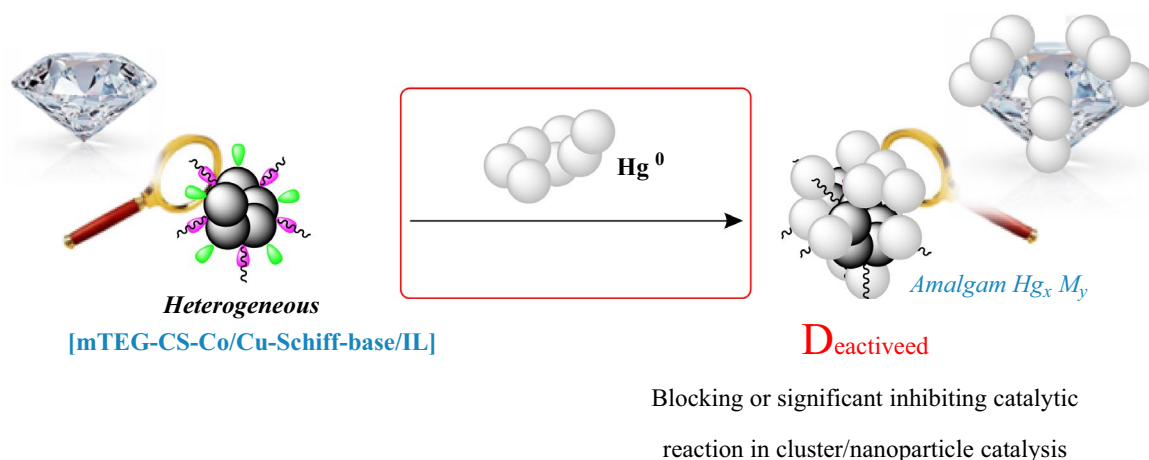


Figure 12. Operational origin of Hg testing in mechanistic studies of catalytic systems.

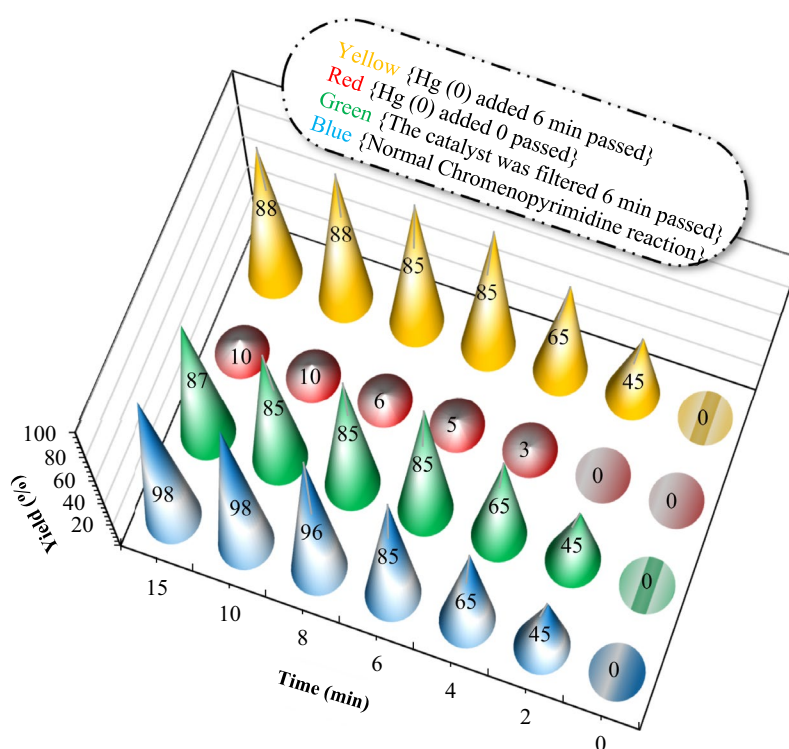


Figure 13. Results of mercury poisoning and hot filtration experiments on the one-pot reaction of chromenopyrimidine of benzyl alcohol with 4-hydroxycoumarin, and urea.

with that of mTEG-CS-Co-Schiff-base/IL and mTEG-CS-Cu-Schiff-base/IL alone, it was observed that the bimetallic nanohybrid exhibits higher catalytic activity. This enhanced catalytic performance can be attributed to the role of cobalt and copper in dispersing the chitosan surface and the synergistic effect between metals. The presence of both cobalt and copper increases the number of active sites available for the catalytic reaction, leading to improved catalytic activity. It should be noted that the objective of this study is to introduce a catalyst with potential applications in enhancing organic reactions. The synthesis of chromenopyrimidine-2,5-dione derivatives serves as a specific model for organic transformation in this context.

Figure 14 proposes a mechanism for the reaction of chromenopyrimidine synthesis using the newly developed hydrophilic heterogeneous cobalt/copper bimetallic catalyst. The mechanism involves the synergistic effect of both cobalt and copper metals in the catalyst to enhance the efficiency of the reaction. The proposed mechanism suggests that both copper and cobalt metals play a role in the oxidation of alcohol to aldehyde. Copper metal, which is present in a higher amount based on ICP analysis, acts as the primary activator, while cobalt metal acts as the electron acceptor. In aerobic conditions, aldehydes are produced from alcohols through dehydration in the presence of copper metal. Then, the cobalt metal in the catalyst activates the urea by forming a bond with

Entry	Catalyst	Time (min)	Reaction condition	Yield (%)	References
1	H ₅ BW ₁₂ O ₄₀	30	Reflux, water	97	30
2	HPA@Methenamine-HNTs	20	Reflux, water	97	31
3	CH ₃ SO ₃ H	30	Ultrasound	80	98
4	HSO ₃ Cl	5	Ultrasound	96	98
5	CH ₃ C ₆ H ₄ SO ₃ H	60	Ultrasound	75	98
6	HPA@HNTs-C	4	Ultrasound	95	99
7	Ag@CDNS-SBA-15	25	Water, 55 °C, 125 W	95	100
8	SDS	360	Water, Reflux, Acetic acid	78	101
9	SLS	300	Water, RT	95	102
10	Copper iodide nanoparticles	50	Solvent-free, 79 °C	92	103
11	mTEG-CS-Co/Cu-Schiff-base/IL	15	H ₂ O, 50 °C	98	This work

Table 4. The comparison of the nanohybrid activity of mTEG-CS-Co/Cu-Schiff-base/IL with previously reported catalysts.

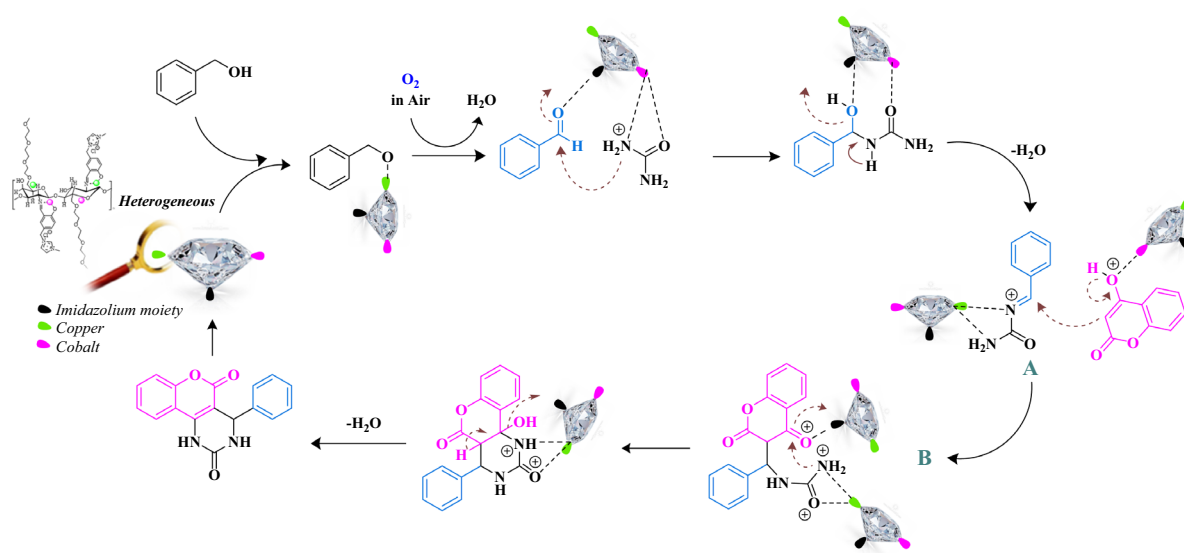


Figure 14. Proposed Mechanism for the Multicomponent TOP Using mTEG-CS-Co/Cu-Schiff-base/IL nanohybrid as a multifunctional catalyst.

the carbonyl and amine group in the compound. This interaction prepares the reaction to proceed and enhances the reactivity of the urea. In this way, cobalt metal as an electron acceptor plays an important role in reducing the electronic potentials of the reaction and increasing the reactivity. In the following, the nanohybrid enables the formation of intermediate (A) by facilitating the Knoevenagel condensation of the aldehydes formed in situ with urea, leading to the synthesis of the imine. Then, the active sites of copper in the catalyst coordinate with the imine group (A) and undergo Michael's addition, which involves the nucleophilic addition of 4-hydroxycoumarin. This results in the formation of intermediate B. Intermediate B undergoes nucleophilic attack of amine to the carbonyl group of 4-hydroxycoumarin. This step leads to the formation of the chromenopyrimidine product after the removal of a water molecule. Finally, the nanohybrid is regenerated for the next run, completing the catalytic cycle. Overall, the proposed mechanism highlights the intricate steps involved in the chromenopyrimidine synthesis and elucidates how the bimetallic catalyst facilitates each stage, providing insight into the catalytic process enabled by the cobalt/copper nanohybrid catalyst (Fig. 14).

Conclusion

The paper describes the development and characterization of a new hydrophilic heterogeneous cobalt/copper bimetallic catalyst for synthesizing chromopyrimidine derivatives. The catalyst composition includes chitosan-Schiff base, imidazolium moieties as ionic liquids, and mono-methoxy triethylene glycol (mTEG) as a phase transfer functional group. This catalyst enables a multicomponent tandem oxidation process starting from alcohols, offering an economically viable and environmentally sustainable alternative to conventional methods. The paper emphasizes several advantages of this process. Firstly, the catalyst is easy to handle and exhibits high reusability, contributing to cost-effectiveness and practicality. Additionally, the reaction time is significantly reduced, leading to shorter overall reaction periods. The work-up process is also simplified, and the yield of the desired

chromopyrimidine derivatives is high. Notably, the use of water as a solvent promotes the eco-friendliness and sustainability of the process. The paper also provides a comprehensive characterization of the catalyst using various techniques such as XRD, FE-SEM, TEM, TGA, FT-IR, EDX-EDS, AFM, NMR, and ICP. Through this comprehensive characterization, the structure, composition, and effectiveness of the catalyst in synthesizing chromopyrimidine derivatives are clearly understood. Overall, the paper presents a promising approach to the synthesis of chromopyrimidine derivatives using a sustainable and eco-friendly process. The development of a new hydrophilic heterogeneous cobalt/copper bimetallic catalyst, along with its detailed characterization, makes a valuable contribution to the fields of medicinal and synthetic chemistry.

Data availability

All data generated or analyzed during this study are included in this published article (and its Supplementary Information files).

Received: 26 July 2023; Accepted: 26 October 2023

Published online: 04 November 2023

References

- Ghamari Kargar, P., Nayebi, M., Parhizi, Z. & Varma, R. S. Nickel nanoparticles adorned on magnetized cellulose nanofibers: ultrasound-facilitated cross coupling reactions. *Cellulose*. **29**, 9183–9198 (2022).
- Ghamari Kargar, P., Ghasemi, M. & Bagherzade, G. Copper (II) supported on a post-modified magnetic pectin Fe_3O_4 @Pectin-Imidazole- SO_3H -Cu(II): an efficient biopolymer-based catalyst for selective oxidation of alcohols with aqueous TBHP. *Sci. Iran*. **29**, 1338–1350 (2022).
- Ghamari Kargar, P., Ravanjamjani, A. & Bagherzade, G. A novel water-dispersible and magnetically recyclable nickel nanoparticles for the one-pot reduction-Schiff base condensation of nitroarenes in pure water. *J. Chinese Chem. Soc.* **68**, 1916–1933 (2021).
- Khashei Siuki, H., Bagherzade, G. & Ghamari Kargar, P. A green method for synthesizing nickel nanoparticles supported by magnetized pectin: Applied as a catalyst for aldehyde synthesis as a precursor in xanthan synthesis. *ChemistrySelect* **5**, 13537–13544 (2020).
- Halimehjani, A. Z., Namboothiri, I. N. N. & Hooshmand, S. E. Part I: Nitroalkenes in the synthesis of heterocyclic compounds. *RSC Adv.* **4**, 48022–48084 (2014).
- Mermer, A., Keles, T. & Sirin, Y. Recent studies of nitrogen containing heterocyclic compounds as novel antiviral agents: A review. *Bioorg. Chem.* **114**, 105076 (2021).
- Ghamari Kargar, P., Noorian, M., Chamani, E., Bagherzade, G. & Kiani, Z. Synthesis, characterization and cytotoxicity evaluation of a novel magnetic nanocomposite with iron oxide deposited on cellulose nanofibers with nickel (Fe_3O_4 @NFC@ONSM-Ni). *RSC Adv.* **11**, 17413–17430 (2021).
- Bakhshi, O., Bagherzade, G. & Ghamari kargar, P. Biosynthesis of organic nanocomposite using Pistacia vera L. hull: an efficient antimicrobial agent. *Bioinorg. Chem. Appl.* **2021**, 1–18 (2021).
- Bagherzade, G., Bakhshi, O. & Ghamarikargar, P. Biosynthesis of organic nanocomposite using Pistacia Vera L. hull: An efficient antimicrobial agent. *Medbiotech J.* **5**, 41–48 (2021).
- Tamilthendral, V., Ramesh, R. & Malecki, J. G. New ruthenium(II) catalysts enable the synthesis of 2-amino-4 H -chromenes using primary alcohols via acceptorless dehydrogenative coupling. *New J. Chem.* **46**, 21568–21578 (2022).
- Mishra, N. P., Satish, L., Mohapatra, S., Nayak, S. & Sahoo, H. A spectroscopic insight into the interaction of chromene 1,2,4-oxadiazole-based compounds with bovine serum albumin. *Res. Chem. Intermed.* **47**, 1181–1195 (2021).
- Khashei Siuki, H., Ghamari Kargar, P. & Bagherzade, G. New Acetamidine Cu(II) Schiff base complex supported on magnetic nanoparticles pectin for the synthesis of triazoles using click chemistry. *Sci. Rep.* **12**, 3771 (2022).
- Shabir, G., Shafique, I. & Saeed, A. Ultrasound assisted synthesis of 5–7 membered heterocyclic rings in organic molecules. *J. Heterocycl. Chem.* **59**, 1669–1702 (2022).
- Katiyar, M. K. *et al.* Synthetic strategies and pharmacological activities of chromene and its derivatives: An overview. *J. Mol. Struct.* **1263**, 133012 (2022).
- Ganyecz, A., Kállay, M. & Csontos, J. Thermochemistry of uracil, thymine, cytosine, and adenine. *J. Phys. Chem. A* **123**, 4057–4067 (2019).
- Hirao, K., Nakajima, T., Chan, B., Song, J.-W. & Bae, H.-S. Core-level excitation energies of nucleic acid bases expressed as orbital energies of the Kohn-Sham density functional theory with long-range corrected functionals. *J. Phys. Chem. A* **124**, 10482–10494 (2020).
- Panday, A. K., Mishra, R., Jana, A., Parvin, T. & Choudhury, L. H. Synthesis of pyrimidine fused quinolines by ligand-free copper-catalyzed domino reactions. *J. Org. Chem.* **83**, 3624–3632 (2018).
- Escobar, A. M., Blustein, G., Luque, R. & Romanelli, G. P. Recent applications of heteropolyacids and related compounds in heterocycle synthesis Contributions between 2010 and 2020. *Catalysts* **11**, 291 (2021).
- Alamgir, A. N. M. Secondary Metabolites: Secondary Metabolic Products Consisting of C and H; C, H, and O; N, S, and P Elements; and O/N Heterocycles. *Phytochem. Bioact. Compd.* **2**, 165–309 (2018).
- Singh, A. K. *et al.* Concept of hybrid drugs and recent advancements in anticancer hybrids. *Pharmaceuticals* **15**, 1071 (2022).
- Kiem, P. V. *et al.* Enantiomeric chromene derivatives with anticancer effects from *Mallotus apelta*. *Bioorg. Chem.* **104**, 104268 (2020).
- Gohil, J. D., Patel, H. B. & Patel, M. P. Synthesis and evaluation of new chromene based [1,8]naphthyridines derivatives as potential antimicrobial agents. *RSC Adv.* **6**, 74726–74733 (2016).
- Dharmapalan, B. T. *et al.* Inhibitory potential of chromene derivatives on structural and non-structural proteins of dengue virus. *Viruses* **14**, 2656 (2022).
- Arif, N. *et al.* Synthesis, spectroscopic, SC-XRD/DFT and non-linear optical (NLO) properties of chromene derivatives. *RSC Adv.* **13**, 464–477 (2023).
- Ryzhkova, Y. E. *et al.* Green electrocatalytic assembling of salicylaldehydes, kojic acid, and malonic acid derivatives into 2-amino-4H-chromenes as potent anti-inflammatory agents. *ChemistrySelect* **7**, (2022).
- Dam, B., Jamatia, R., Gupta, A. & Pal, A. K. Metal-free greener syntheses of pyrimidine derivatives using a highly efficient and reusable graphite oxide carbocatalyst under solvent-free reaction conditions. *ACS Sustain. Chem. Eng.* **5**, 11459–11469 (2017).
- Santhoshkumar, R. & Cheng, C. Reaching green: Heterocycle synthesis by transition metal-catalyzed C–H functionalization in sustainable medium. *Chem. A Eur. J.* **25**, 9366–9384 (2019).
- Morja, M. I., Moradiya, R. B. & Chikhaliya, K. H. First-row transition metal for isocyanide-involving multicomponent reactions (IMCR). *Mol. Divers.* 1–40 (2022).

29. Alblewi, F. F. *et al.* Antiproliferative effect, cell cycle arrest and apoptosis generation of novel synthesized anticancer heterocyclic derivatives based 4H-benzo[h]chromene. *Bioorg. Chem.* **87**, 560–571 (2019).
30. Reheim, M. A. M. A., Hafiz, I. S. A. & Elian, M. A. Synthesis and antimicrobial evaluation of some novel pyrimidine, pyrazole, chromene and tetrahydrobenzo[b]thiophene derivatives bearing pyrimidinthione moiety. *Curr. Org. Synth.* **17**, 548–557 (2020).
31. Heravi, M. M., Hosseinejad, T., Tamimi, M., Zadsirjan, V. & Mirzaei, M. 12-Tungstoboric acid ($H_2BW_{12}O_{40}$) as an efficient Lewis acid catalyst for the synthesis of chromenopyrimidine-2,5-diones and thioxochromenopyrimidin-5-ones: Joint experimental and computational study. *J. Mol. Struct.* **1205**, 127598 (2020).
32. Sadjadi, S., M. Heravi, M., Zadsirjan, V., Beheshtiha, S. Y. S. & Kelishadi, R. R. HPA@Methenamine-HNTs: A novel catalyst for promoting one-pot and three-component synthesis of chromenopyrimidine-2,5-diones and thioxochromenopyrimidin-5-ones in aqueous media. *ChemistrySelect* **3**, 12031–12038 (2018).
33. Mehrabi, H. & Baniasad-Dashtabi, M. One-pot synthesis of novel heterocyclic chromenopyrimidine-2,5-dione and thioxochromenopyrimidin-5-one derivatives. *J. Chem. Res.* **39**, 294–295 (2015).
34. Ghamari Kargar, P., Aryanejad, S. & Bagherzade, G. Simple synthesis of the novel Cu-MOF catalysts for the selective alcohol oxidation and the oxidative cross-coupling of amines and alcohols. *Appl. Organomet. Chem.* **34**, (2020).
35. Ghamari kargar, P., Bagherzade, G. & Beyzaei, H. A porous metal-organic framework (Ni-MOF): An efficient and recyclable catalyst for cascade oxidative amidation of alcohols by amines under ultrasound-irradiations. *Mol. Catal.* **526**, 112372 (2022).
36. Ciriminna, R., Pandarus, V., Béland, F., Xu, Y.-J. & Pagliaro, M. Heterogeneously catalyzed alcohol oxidation for the fine chemical industry. *Org. Process Res. Dev.* **19**, 1554–1558 (2015).
37. Lang, X.-D. & He, L.-N. Green catalytic process for cyclic carbonate synthesis from carbon dioxide under mild conditions. *Chem. Rec.* **16**, 1337–1352 (2016).
38. Ireland, R. E., Armstrong, J. D., Lebreton, J., Meissner, R. S. & Rizzacasa, M. A. Convergent synthesis of polyether ionophore antibiotics: synthesis of the spiroketal and tricyclic glycol segments of monensin. *J. Am. Chem. Soc.* **115**, 7152–7165 (1993).
39. Jeena, V. & Robinson, R. S. The 'Ireland' one-pot alcohol oxidation coupling reactions: celebrating 30 years of diverse synthesis. *Org. Biomol. Chem.* **13**, 8958–8977 (2015).
40. Alirezvani, Z., Dekamin, M. G. & Valiey, E. Cu(II) and magnetite nanoparticles decorated melamine-functionalized chitosan: A synergistic multifunctional catalyst for sustainable cascade oxidation of benzyl alcohols/Knoevenagel condensation. *Sci. Rep.* **9**, 17758 (2019).
41. Ch, V., Sandupatla, R., Lingareddy, E. & Raju, D. One-pot synthesis of imines by direct coupling of alcohols and amines over magnetically recoverable $CdFe_2O_4$ nanocatalyst. *Mater. Lett.* **302**, 130417 (2021).
42. Bakherad, M. *et al.* Silica-anchored Cu(I) aminothiophenol complex: An efficient heterogeneous catalyst for synthesis of 1,4-disubstituted 1,2,3-triazoles in water. *Iran. J. Catal.* **8**, 179–187 (2018).
43. Ghamari kargar, P. & Bagherzade, G. The anchoring of a Cu(II)-salophen complex on magnetic mesoporous cellulose nanofibers: Green synthesis and an investigation of its catalytic role in tetrazole reactions through a facile one-pot route. *RSC Adv.* **11**, 19203–19220 (2021).
44. Bagherzade, G., Khashei Siuki, H. & Ghamari kargar, P. Use of pectin as a suitable substrate for catalyst synthesis $Fe_3O_4@Pectin@Ni(II)$ and its application in oxidation reaction. *Medbiotech J.* **5**, 1–8 (2021).
45. Faisca Phillips, A. M., Pombeiro, A. J. L. & Kopylovich, M. N. Recent advances in cascade reactions initiated by alcohol oxidation. *ChemCatChem.* **9**, 217–246 (2017).
46. Ghamari kargar, P., Bagherzade, G. & Eshghi, H. Novel biocompatible core/shell $Fe_3O_4@NFC@Co(II)$ as a new catalyst in a multicomponent reaction: An efficient and sustainable methodology and novel reusable material for one-pot synthesis of 4 H-pyran and pyranopyrazole in aqueous media. *RSC Adv.* **10**, 37086–37097 (2020).
47. Ghamari kargar, P., Bagherzade, G. & Ghasemi, M. Magnetic nanoparticles embedded in pectin-based as an environmentally friendly recyclable nanocatalyst. *Medbiotech J.* **5**, 9–14 (2021).
48. Zheng, J. *et al.* Visualization of Zika virus infection via a light-initiated bio-orthogonal cycloaddition labeling strategy. *Front. Bioeng. Biotechnol.* **10**, (2022).
49. Ghani, M. *et al.* Synthesis of cellulose nanofibers-based $ImSalophen@Fe_3O_4$ as a green sorbent for magnetic solid-phase extraction of chlorophenols followed by quantification via high-performance liquid chromatography-ultraviolet detection. *Microchem. J.* **187**, 108368 (2023).
50. Ghamari kargar, P., Bakhshi, F. & Bagherzade, G. Value-added synthesized acidic polymer nanocomposite with waste chicken eggshell: A novel metal-free and heterogeneous catalyst for Mannich and hantzsch cascade reactions from alcohols. *Arab. J. Chem.* **16**, 104564 (2023).
51. Munir, A. *et al.* Metal nanoclusters: New paradigm in catalysis for water splitting, solar and chemical energy conversion. *ChemSusChem* **12**, 1517–1548 (2019).
52. Porcheddu, A., Colacino, E., De Luca, L. & Delogu, F. Metal-mediated and metal-catalyzed reactions under mechanochemical conditions. *ACS Catal.* **10**, 8344–8394 (2020).
53. Meninno, S. Valorization of waste: Sustainable organocatalysts from renewable resources. *ChemSusChem.* **13**, 439–468 (2020).
54. Shah, S. S. *et al.* Present status and future prospects of jute in nanotechnology: A review. *Chem. Rec.* **21**, 1631–1665 (2021).
55. Lai, S., Gao, J., Zhang, H., Cheng, L. & Xiong, X. Luffa sponge supported dendritic imidazolium IIs with high-density active sites as highly efficient and environmentally friendly catalysts for CO_2 chemical fixation. *J. CO₂ Util.* **38**, 148–157 (2020).
56. Zakhireh, S. *et al.* Bioactive chitosan-based organometallic scaffolds for tissue engineering and regeneration. *Top. Curr. Chem.* **380**, 13 (2022).
57. Youssef, A. M. & El-Sayed, S. M. Bionanocomposites materials for food packaging applications: Concepts and future outlook. *Carbohydr. Polym.* **193**, 19–27 (2018).
58. Jawad, A. H. & Abdulhameed, A. S. Facile synthesis of crosslinked chitosan-tripolyphosphate/kaolin clay composite for decolorization and COD reduction of remazol brilliant blue R dye: Optimization by using response surface methodology. *Colloids Surf. A Physicochem. Eng. Asp.* **605**, 125329 (2020).
59. Chen, C., Xi, Y. & Weng, Y. Recent advances in cellulose-based hydrogels for tissue engineering applications. *Polymers (Basel).* **14**, 3335 (2022).
60. Anju, S., Ashtami, J. & Mohanan, P. V. Black phosphorus, a prospective graphene substitute for biomedical applications. *Mater. Sci. Eng. C* **97**, 978–993 (2019).
61. Rohaizad, N., Mayorga-Martinez, C. C., Fojtů, M., Latiff, N. M. & Pumera, M. Two-dimensional materials in biomedical, bio-sensing and sensing applications. *Chem. Soc. Rev.* **50**, 619–657 (2021).
62. El-Aswar, E. I., Ramadan, H., Elkik, H. & Taha, A. G. A comprehensive review on preparation, functionalization and recent applications of nanofiber membranes in wastewater treatment. *J. Environ. Manage.* **301**, 113908 (2022).
63. Chadha, U. *et al.* Retracted: Advances in chitosan biopolymer composite materials: from bioengineering, wastewater treatment to agricultural applications. *Mater. Res. Express.* **9**, 052002 (2022).
64. Shariatinia, Z. Pharmaceutical applications of chitosan. *Adv. Colloid Interface Sci.* **263**, 131–194 (2019).
65. Al-Tayyar, N. A., Youssef, A. M. & Al-hindi, R. Antimicrobial food packaging based on sustainable Bio-based materials for reducing foodborne Pathogens: A review. *Food Chem.* **310**, 125915 (2020).
66. Rostamabadi, H., Assadpour, E., Tabarestani, H. S., Falsafi, S. R. & Jafari, S. M. Electrospinning approach for nanoencapsulation of bioactive compounds; recent advances and innovations. *Trends Food Sci. Technol.* **100**, 190–209 (2020).

67. Zhang, L., Luo, H., Liu, P., Fang, W. & Geng, J. A novel modified graphene oxide/chitosan composite used as an adsorbent for Cr(VI) in aqueous solutions. *Int. J. Biol. Macromol.* **87**, 586–596 (2016).
68. Gawande, M. B., Bonifácio, V. D. B., Luque, R., Branco, P. S. & Varma, R. S. Benign by design: catalyst-free in-water, on-water green chemical methodologies in organic synthesis. *Chem. Soc. Rev.* **42**, 5522 (2013).
69. Chanda, A. & Fokin, V. V. Organic synthesis “on water”. *Chem. Rev.* **109**, 725–748 (2009).
70. Vekariya, R. L. A review of ionic liquids: Applications towards catalytic organic transformations. *J. Mol. Liq.* **227**, 44–60 (2017).
71. Li, S. *et al.* Template-free fabrication of magnetic mesoporous poly(ionic liquid)s: Efficient interfacial catalysts for hydrogenation reaction and transesterification of soybean oil. *J. Mater. Chem. A.* **10**, 3531–3542 (2022).
72. Yu, Y.-Y. *et al.* Synergistic catalysis: A powerful new strategy for the production of lignin-derived aromatic monomers. *Fuel Process. Technol.* **235**, 107388 (2022).
73. Gupta, R. *et al.* Magnetically supported ionic liquids: a sustainable catalytic route for organic transformations. *Mater. Horizons.* **7**, 3097–3130 (2020).
74. Hallett, J. P. & Welton, T. Room-temperature ionic liquids: Solvents for synthesis and catalysis. 2. *Chem. Rev.* **111**, 3508–3576 (2011).
75. Lu, X. *et al.* Novel photic and magnetic double responsive Pickering interfacial solid catalysts for biodiesel production. *Fuel* **310**, 122318 (2022).
76. Zheng, W. *et al.* Ionic liquid-functionalized graphene oxide as an efficient support for the chiral salen Mn(III) complex in asymmetric epoxidation of unfunctionalized olefins. *Catal. Sci. Technol.* **5**, 2092–2102 (2015).
77. Srinivas Reddy, A. & Laali, K. K. Sonogashira cross-coupling in a designer ionic liquid (IL) without copper, external base, or additive, and with recycling and reuse of the IL. *Tetrahedron Lett.* **56**, 4807–4810 (2015).
78. Cano, I. *et al.* Paramagnetic ionic liquid-coated SiO₂@Fe₃O₄ nanoparticles-The next generation of magnetically recoverable nanocatalysts applied in the glycolysis of PET. *Appl. Catal. B Environ.* **260**, 118110 (2020).
79. Zarnegar, Z. & Safari, J. Heterogenization of an imidazolium ionic liquid based on magnetic carbon nanotubes as a novel organocatalyst for the synthesis of 2-amino-chromenes via a microwave-assisted multicomponent strategy. *New J. Chem.* **40**, 7986–7995 (2016).
80. Ghamari kargar, P., Bagherzade, G. & Eshghi, H. Design and synthesis of magnetic Fe₃O₄@NFC-ImSalophCu nanocatalyst based on cellulose nanofibers as a new and highly efficient, reusable, stable and green catalyst for the synthesis of 1,2,3-triazoles. *RSC Adv.* **10**, 32927–32937 (2020).
81. Teimuri-Mofrad, R., Esmati, S., Tahmasebi, S. & Gholamhosseini-Nazari, M. Bisferrocene-containing ionic liquid supported on silica coated Fe₃O₄: A novel nanomagnetic catalyst for the synthesis of dihydropyrano[2,3- c]coumarin derivatives. *J. Organomet. Chem.* **870**, 38–50 (2018).
82. Neysi, M., Elhamifar, D. & Norouzi, M. Ionic liquid functionalized magnetic organosilica nanocomposite: A powerful and efficient support for manganese catalyst. *Mater. Chem. Phys.* **243**, 122589 (2020).
83. Hamadi, H., Kooti, M., Afshari, M., Ghiasifar, Z. & Adibpour, N. Magnetic nanoparticle supported polyoxometalate: An efficient and reusable catalyst for solvent-free synthesis of α -aminophosphonates. *J. Mol. Catal. A Chem.* **373**, 25–29 (2013).
84. Shirzaei, M., Mollashahi, E., TaherMaghsoudlou, M. & Lashkari, M. Novel synthesis of silica-coated magnetic nano-particles based on acidic ionic liquid, as a highly efficient catalyst for three component system leads to furans derivatives. *J. Saudi Chem. Soc.* **24**, 216–222 (2020).
85. Zolfigol, M. A., Ayazi-Nasrabadi, R. & Bagheri, S. The first urea-based ionic liquid-stabilized magnetic nanoparticles: An efficient catalyst for the synthesis of bis(indolyl)methanes and pyrano[2,3-d]pyrimidinone derivatives. *Appl. Organomet. Chem.* **30**, 273–281 (2016).
86. Nguyen, H. T., Le Thi, N.-P., Nguyen Chau, D.-K. & Tran, P. H. New nano-Fe₃O₄-supported Lewis acidic ionic liquid as a highly effective and recyclable catalyst for the preparation of benzoxanthenes and pyrroles under solvent-free sonication. *RSC Adv.* **8**, 35681–35688 (2018).
87. Aalam, M. J. *et al.* DABCO-based chiral ionic liquids as recoverable and reusable organocatalyst for asymmetric Diels-Alder reaction. *Chirality* **34**, 134–146 (2022).
88. Nayebe, M. *et al.* TiO₂/g-C₃N₄/SO₃H(IL): Unique usage of ionic liquid-based sulfonic acid as an efficient photocatalyst for visible-light-driven preparation of 5-HMF from cellulose and glucose. *ACS Appl. Mater. Interfaces.* **15**, 8054–8065 (2023).
89. Ghamari Kargar, P. & Bagherzade, G. A Green synthesis strategy of binuclear catalyst for the C-C cross-coupling reactions in the aqueous medium: Hiyama and Suzuki–Miyaura reactions as case studies. *Front. Chem.* **9**, (2021).
90. Hajipour, A. R., Rezaei, F. & Khorsandi, Z. Pd/Cu-free Heck and Sonogashira cross-coupling reaction by Co nanoparticles immobilized on magnetic chitosan as reusable catalyst. *Green Chem.* **19**, 1353–1361 (2017).
91. Ghamari kargar, P. & Bagherzade, G. The anchoring of a Cu(II)–salophen complex on magnetic mesoporous cellulose nanofibers: Green synthesis and an investigation of its catalytic role in tetrazole reactions through a facile one-pot route. *RSC Adv.* **11**, 19203–19220 (2021).
92. GhamariKargar, P. & Bagherzade, G. Robust, highly active, and stable supported Co(II) nanoparticles on magnetic cellulose nanofiber-functionalized for the multi-component reactions of piperidines and alcohol oxidation. *RSC Adv.* **11**, 23192–23206 (2021).
93. Ghamari kargar, P., Bagherzade, G., Beyzaei, H. & Arghavani, S. BioMOF-Mn: An antimicrobial agent and an efficient nanocatalyst for domino one-pot preparation of xanthene derivatives. *Inorg. Chem.* **61**, 10678–10693 (2022).
94. Ghamari kargar, P., Bagherzade, G. & Eshghi, H. Introduction of a trinuclear manganese(III) catalyst on the surface of magnetic cellulose as an eco-benign, efficient and reusable novel heterogeneous catalyst for the multi-component synthesis of new derivatives of xanthene. *RSC Adv.* **11**, 4339–4355 (2021).
95. Thombal, P. R., Thombal, R. S. & Han, S. S. Chitosan-derived N-doped carbon catalysts with a metallic core for the oxidative dehydrogenation of NH–NH bonds. *RSC Adv.* **10**, 474–481 (2020).
96. Hongfeng, Z., El-Kott, A., Ezzat Ahmed, A. & Khames, A. Synthesis of chitosan-stabilized copper nanoparticles (CS-Cu NPs): Its catalytic activity for C-N and C-O cross-coupling reactions and treatment of bladder cancer. *Arab. J. Chem.* **14**, 103259 (2021).
97. Adewuyi, S., Bisiriyu, I. O., Akinremi, C. A. & Amolegbe, S. A. Synthesis, spectroscopic, surface and catalytic reactivity of chitosan supported Co(II) and Its Zerovalentcobalt Nanobiocomposite. *J. Inorg. Organomet. Polym. Mater.* **27**, 114–121 (2017).
98. A.M. Al-Kadasi, G. M. N. A facile and efficient ultrasound-assisted chlorosulfonic acid catalyzed one-pot synthesis of benzopyranopyrimidines under solvent-free conditions. *J. Chem. Pharm. Res.* **2013**, 204–210 (2013).
99. Sadjadi, S., Heravi, M. M. & Malmir, M. Heteropolyacid@creatin-halloysite clay: an environmentally friendly, reusable and heterogeneous catalyst for the synthesis of benzopyranopyrimidines. *Res. Chem. Intermed.* **43**, 6701–6717 (2017).
100. Sadjadi, S., Heravi, M. M. & Malmir, M. Bio-assisted synthesized Ag(0) nanoparticles immobilized on SBA-15/cyclodextrin nanosponge adduct: Efficient heterogeneous catalyst for the ultrasonic-assisted synthesis of benzopyranopyrimidines. *Appl. Organomet. Chem.* **32**, e4286 (2018).
101. H. Mehrabi, M. B.-D. One-pot synthesis of novel heterocyclic chromenopyrimidine-2, 5-dione and thioxochromenopyrimidin-5-one derivatives. *J. Chem. Res.* **39**, 294–295 (2015).
102. Sahu, P. K. *et al.* One-pot facile and mild construction of densely functionalized pyrimidines in water via consecutive C-C and C-S bonds formation. *RSC Adv.* **8**, 33952–33959 (2018).

103. Abdolmohammadi, S. & Karimpour, S. Rapid and mild synthesis of quinazolinones and chromeno[d]pyrimidinones using nanocrystalline copper(I) iodide under solvent-free conditions. *Chinese Chem. Lett.* **27**, 114–118 (2016).

Acknowledgements

We gratefully acknowledge the support of this work by the University of Birjand.

Author contributions

P.G.K. Conceptualization, Supervision, Investigation, Writing–original draft. G.B. Project administration, Supervision.

Competing interests

The authors declare no competing interests.

Additional information

Supplementary Information The online version contains supplementary material available at <https://doi.org/10.1038/s41598-023-46004-3>.

Correspondence and requests for materials should be addressed to G.B.

Reprints and permissions information is available at www.nature.com/reprints.

Publisher's note Springer Nature remains neutral with regard to jurisdictional claims in published maps and institutional affiliations.



Open Access This article is licensed under a Creative Commons Attribution 4.0 International License, which permits use, sharing, adaptation, distribution and reproduction in any medium or format, as long as you give appropriate credit to the original author(s) and the source, provide a link to the Creative Commons licence, and indicate if changes were made. The images or other third party material in this article are included in the article's Creative Commons licence, unless indicated otherwise in a credit line to the material. If material is not included in the article's Creative Commons licence and your intended use is not permitted by statutory regulation or exceeds the permitted use, you will need to obtain permission directly from the copyright holder. To view a copy of this licence, visit <http://creativecommons.org/licenses/by/4.0/>.

© The Author(s) 2023